Radar Transparency and Paint Compatibility

A Study of Automobile Bumper and Bumper-Skin Complex Permittivities for 77GHz Microwaves

by

Erik P. Emilsson

Diploma work No. 201/2017
at Department of Materials and Manufacturing Technology
CHALMERS UNIVERSITY OF TECHNOLOGY
Gothenburg, Sweden

Diploma work in the Master Programme Applied Physics

Performed at:	Volvo Cars Sverige AB 405 31 Göteborg, Sweden
Supervisor(s):	Cecilia Wieslander, Martin Emanuelsson, and Kristoffer Lund Volvo Car Sverige AB 405 31 Göteborg, Sweden
Examiner:	Lars Nyborg Department of Materials and Manufacturing Technology Chalmers University of Technology, SE - 412 96 Gothenburg

Radar Transparency and Paint Compatibility
A Study of Automobile Bumper and Bumper-Skin Complex Permittivities for 77GHz Microwaves
Erik P. Emilsson

Diploma work no 201/2017
Department of Materials and Manufacturing Technology
Chalmers University of Technology
SE-412 96 Gothenburg
Sweden
Telephone + 46 (0)31-772 1000

[Chalmers reproservice]
Gothenburg, Sweden 2017

Radar Transparency and Paint Compatibility
A Study of Automobile Bumper and Bumper-Skin Complex Permittivities for 77GHz Microwaves
Erik P. Emilsson
Department of Materials and Manufacturing Technology
Chalmers University of Technology

SUMMARY

This study aims to identify the key factors, regarding bumper and bumper coatings, that affect radar transparency for radar at 77GHz. Dielectric spectroscopy in the 60-90GHz microwave region was performed using the free-space method was performed on 21 flat plastic substrates with various combinations of primers, basecoats and topcoats. 4 additional plates were repainted to simulate aftermarket paint. The substrates were PP-blends and some of the basecoats had effect pigments such as aluminum metal flakes, mica and Xiralic. The samples were received from a Volvo Cars supplier, so there is limited information of the composition of plastic substrates and coatings available.

The free space method was done using a two-port network analyzer. Time-domain clipping and normalization was done on the S-parameters. Complex permittivities for each plastic substrate and coating were calculated from the curve fitting values of a multi-layer dielectric model. Both the obtained radar measurements and thickness measurements were required for the calculation of the permittivities.

Thickness measurements were done on the cross-sections of all cut samples using an optical microscope. Effect pigments were observed in both optical microscope and SEM. FT-IR spectroscopy was done on the plastic substrates to obtain information on the compositions. TGA was done on the plastic substrates to measure polymer matrix and filler concentrations. DCS was done on the plastic substrates percent crystallinity was calculated using a reference value for the enthalpy of 100% crystallinity for Polypropylene, after deducting the fillers.

The results from the materials analyses were compared to the calculated permittivities. Reflection losses, were modeled with MATLAB to show the approximate permittivities of the aftermarket basecoats that were difficult to perform curve fittings on. Metal flake content correlated to a greater real permittivity of the basecoats. A non-metallic effect pigment in similar concentrations as the metal flakes also increased real and imaginary permittivity in a basecoat. Talc, and likely carbon black, also increased real permittivity. MATLAB was also used to show that plastic substrate thickness is to minimize unwanted reflections in radar, as well as a low permittivity for the basecoat.

Keywords: microwave, 77GHz, polymer, dielectric, permittivity, free-space method, metal flakes, effect pigment.

Preface

In this study, the effect of different plastic fillers and coatings, mimicking automobile bumpers and bumper skins, for 77GHz radar has been studied. The Master's Thesis was done in the spring term of 2017, and it was carried out with Jennie Lodén, from KTH, as an unofficial thesis partner. The work performed in Volvo Cars with supervisors Cecilia Wieslander, Martin Emanuelsson and Kristoffer Lund. Lars Nyborg from Chalmers was the examiner for the project.

Tests were carried out in the Material Center and Surface Treatment Department at Volvo Cars in Torslanda. The sample plates were received from a supplier and radar tests were performed in conjunction with another company specializing in radar systems.

I would like to thank my supervisors at Volvo Cars for their support and encouragement. I would like to thank Jennie Lodén for being an excellent thesis partner throughout the whole project. I would also like to thank Annika Hannebäck, Konrad Tarka, Jesper Alm, Iman Vakili, Anna-Karin Uveborn, and Britta Mattsson for their time, help, and expertise in the various areas of technical knowledge required for this project. I would like to thank Lars Nyborg for volunteering to be the examiner and Nasa Panida for being the opponent to the project. Finally, I want to give my appreciation to the numerous people not mentioned who played a role in the success of this project in one way or another.

Contents

1 Introduction

As radars become more prevalent in automobiles, there is a requirement for a greater awareness of how materials interact with radar at microwave frequencies for automobile manufacturers and aftermarket services. If the current trend [1] continues, drivers will rely more on its functions and it will become increasingly crucial that it doesn't fail. Materials and coatings on bumper skins that interfere with the radars can therefore pose a danger to drivers, passengers and pedestrians. This study will investigate how plastic bumpers and their coatings affect radar transparency.

1.1 Background

Radar (Radar Detection and Ranging) in cars has seen use on roads and highways since the early 1970's [2]. As opposed to ultrasound, which is mainly used by parking sensors to detect objects in close proximity, radar can also be used to detect traffic dangers on roads and highways at higher speeds. A decrease in radar signal resolution, due to

1. an increase in cars manufactured with radars on the roads and highways,
2. the EU recently switching from allowing automobile radars in the K-band (around 24 GHz) to the more sensitive E-band (around 77-81 GHz) [3],
3. the demand for novel colors and effects for automobile chassis that have a potentially negative effect on signal quality,

has increased awareness for the attenuating and reflective effects of bumper materials and paint. The frequency used by VCC automobile radar is in the range of 77GHz.

Volvo Car Corporation (VCC) automobiles, as well as other automobile companies, have their radar systems attached behind the car bumpers such that the bumper essentially becomes the radome (the radar device's protective layer against the environment). The bumpers are made of composite plastics covered with lacquer and paint. To fully understand the degradation of the radar signals passing through the bumpers it is of importance to study all its materials properties and design aspects. The diagram in *Figure 1* below shows a general outline of plastic, paint and lacquer in the plates to be studied. The polymer, or composite, substrate is in front of the radar. The basecoat can be made of different pigments and/or effect pigments, such as metal flakes and pearlescent pigments. The clearcoat provides protection to the basecoat and improves the longevity of the paint.

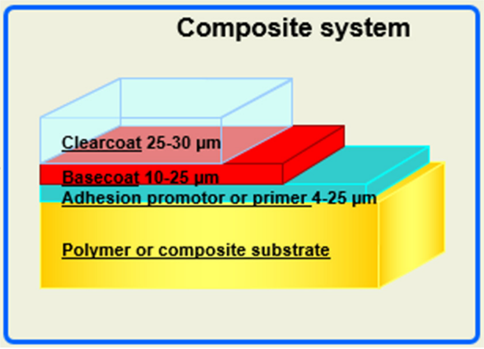

Figure 1: Example of approximate layer thicknesses polymer substrates [4].

1.2 Aim

This thesis will seek to investigate the effects of several types of plastic substrate, paint and lacquer on radar transparency for the 77Ghz frequency, as well as their respective thicknesses. The normal incidence reflected and transmitted signals from a radar in an automobile are i.e. functions of: 1) The dielectric constants of each material, 2) The thicknesses of the materials, and 3) The frequency of the electromagnetic radiation [5]. Therefore, this study will aim at calculating the dielectric constants for each material, the thicknesses of the materials, and the composition of the materials so that the effects of the materials on radar reflection and transmission can be compared.

Additionally, this thesis is to be the first step for Volvo Cars to produce a reliable method for classification of plastics and coatings for future studies in radar transparency.

1.3 Scope

21 sample configurations with several types and variations of paints and lacquer are provided from a bumper materials supplier to Volvo Cars. These samples have the same configurations as bumpers painted for cars in production. 4 additional sample configurations are provided by Volvo Cars to simulate aftermarket “repainted” bumpers. This project will seek to gain data from the 25 plates only, even if the results show that a certain factor in these plates requires further investigation to fully understand. For example, a detailed relationship between the orientations and types of metal flakes and the dielectric constant might be of interest based on the literature study [6].

Dielectric spectroscopy measurements for normal incidence electromagnetic radiation, thickness measurements using optical microscope, and materials analysis with various methods will be done on all sample configurations. There will unfortunately be limited information from the company on the composition of the plastic substrates, paints and lacquer. Therefore, a thorough materials analysis is required on all the samples to determine the effects of materials aspects on radar. DSC, TGA, EDX, and FT-IR are used in this study, but XRD and gas chromatography can also be used to produce results in this type of study [7]. However, due to time-constraints and focus on the most relevant variables, only the former were used.

In a production vehicle, the radar sits behind a concave bumper, rather than a flat one such as the sample plates that were studied in this project. The angle of incidence is of relevance in dielectric spectroscopy, as will be shown in a later section about dielectric materials. However, measuring the angle as a function of radar reflection and transparency is not in the scope of this study.

Reflected radar waves traveling through the layers produce interference with each other. It is of interest to minimize the reflected signal to produce a signal with higher resolution. Thus, finding the real dielectric constants of the layers will be needed to propose optimal thicknesses for the design of bumpers.

Due to the reflective properties of the metal flakes in some of the basecoats, it is reasonable to expect that the metal flakes will have a noticeable effect on the imaginary part of the dielectric constant. Aftermarket paints have a higher concentration of metal flakes, and it is therefore of interest to know how much of an effect metal flakes have on the radar transparency. By comparing the paints that have metal flakes from the supplier of factory paints and the aftermarket paints, there should be enough information to get an idea of the effects of metal flake concentration on the complex part of the dielectric constant.

The dielectric constant of the plastic substrate is also of interest. A rough idea of how the type and concentration of talc and carbon black in the plastic substrate affect the absorption of the radar signal is of interest, as well as the level of crystallinity of the plastic. The results of the radar measurements at different plastic thicknesses will provide necessary information to make conclusions on the dielectric constant of this layer. The dielectric constant of the primer and clearcoat are not expected to be very high, but are nonetheless important to analyze.

2 Theory

2.1 Electromagnetism and dielectrics

An understanding of how electromagnetic radiation interacts with materials is critical to extracting data from dielectric spectroscopy measurements. Furthermore, the simplifications and assumptions made in our measurements may not always apply with other materials or with other methods.

2.1.1. Dielectric materials

The equations that describe the nature of electromagnetic waves in space, assuming no sources of radiation [5], are Maxwell's equations:

$$\begin{aligned} \vec{\nabla} \cdot \vec{E} &= 0 \\ \vec{\nabla} \cdot \vec{B} &= 0 \\ \vec{\nabla} \times \vec{E} &= -\frac{\partial \vec{B}}{\partial t} \\ \nabla \times \vec{H} &= -\frac{\partial \vec{D}}{\partial t} \end{aligned}$$

The constitutive relations describe how electromagnetic waves traveling in a material (dielectric) will change E and the B fields. For a homogeneous, isotropic dielectric, they are simply:

$$\begin{aligned} \vec{D} &= \varepsilon \vec{E} \\ \vec{B} &= \mu \vec{H} \end{aligned}$$

where the permittivity and permeability in a dielectric are, respectively,

$$\begin{aligned} \varepsilon &= \varepsilon_0 (1 + \chi) \\ \mu &= \mu_0 (1 + \chi_m) \end{aligned}$$

Where ε and μ are the permittivity and the permeability of the materials, ε_0 and μ_0 are the free space permittivity and permeability, and χ and χ_m are the electric and magnetic susceptibilities. It is common to set the permeability equal to the free space permeability, $\mu = \mu_0$ [5], meaning the the materials studied are non-magnetic. Thus, the only factor that contributes to a difference in electromagnetic radiation as it travels through a dielectric is ε. However, the dielectric constant is linked to the refracitve index [8]:

$$n = \sqrt{\frac{\varepsilon}{\varepsilon_0} \frac{\mu}{\mu_0}} \approx \sqrt{\frac{\varepsilon}{\varepsilon_0}}$$

This means that materials with different permittivities will reflect some of the incident radiation at their interface. For isotropic dielectrics, the reflected and transmitted radiation will not depend on the polarization of the incident radiation. However, for anisotropic media, a dielectric tensor for permittivity is used to describe the change in radiation instead of a simple value:

$$\begin{bmatrix} \overrightarrow{D_x} \\ \overrightarrow{D_y} \\ \overrightarrow{D_z} \end{bmatrix} = \begin{bmatrix} \varepsilon_{xx} & \varepsilon_{xy} & \varepsilon_{xz} \\ \varepsilon_{yx} & \varepsilon_{yy} & \varepsilon_{yz} \\ \varepsilon_{zx} & \varepsilon_{zy} & \varepsilon_{zz} \end{bmatrix} \begin{bmatrix} \overrightarrow{E_x} \\ \overrightarrow{E_y} \\ \overrightarrow{E_z} \end{bmatrix}$$

In other words, there is a different dielectric tensor in each spatial direction, meaning a different index of refraction at each spatial direction, leading to different values of reflected and transmitted radiaton for different polarizations of incident radiation. In our study we make the assumption that we have isotropic. Thus, we will not be investigating the effect of radiation with different polarizations. Furthermore, we make the assumption that the material is always homogeneous when estimating the dielectric, even though it is obvious that it is not always the case, as with effect pigments and metal flakes in some of the base coat of our samples.

In addition to a reflection term at the boundary, an additional term representing the absorption of radiation traveling through the dielectric is required. It is common to write the permittivity as:

$$\varepsilon = \varepsilon' - i\varepsilon''$$

Where the real term ε' is representative of the index of refraction, and ε'' is representative of the losses of the wave when traveling through the dielectric. The negative sign is due to a sign convention. Figure 2 shows graphically how the real and imaginary parts of the permittivity affect electromagnetic radiation in a dielectric.

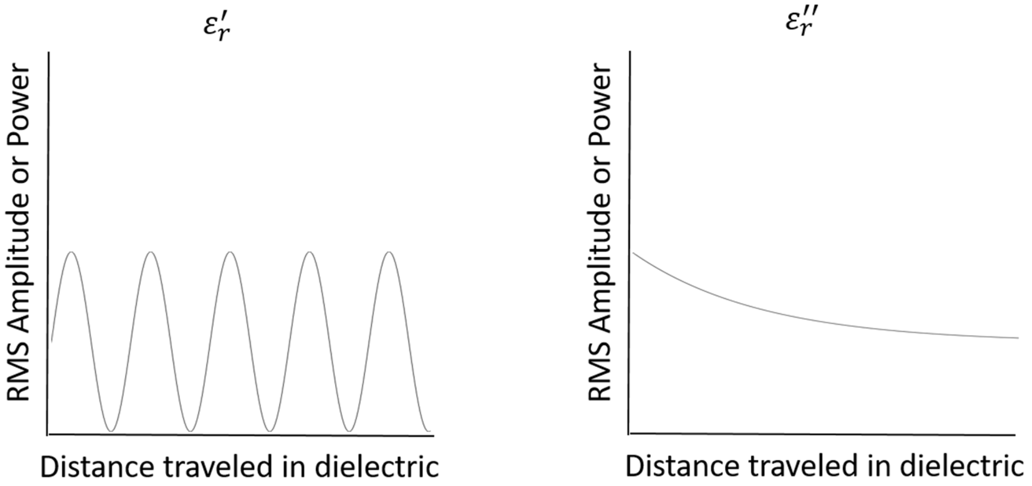

Figure 2: Graphical representation of a purely real dielectric constant (to the right) and a purely imaginary dielectric constant (to the left), in a dielectric. In practice, dielectrics have both a real and imaginary part.

There is also a connection between the permittivity and the response of the material to electromagnetic radiation. The polarization in the material is written as:

$$\vec{P} = \varepsilon_0 \varepsilon \vec{E}$$

Using the polarization and the Drude-Lorentz mode [5], a relationship between frequency and dielectric constant can be derived. This model shows that there is a heavy dependence between the two variables. In other words, the permittivity can vary greatly between different frequencies. For example, other studies have shown that at microwave frequencies under 77GHz, both aluminum and carbon black fillers have a much greater effect on a composite's permittivity [9] [10].

2.1.2. Boundary between dielectrics

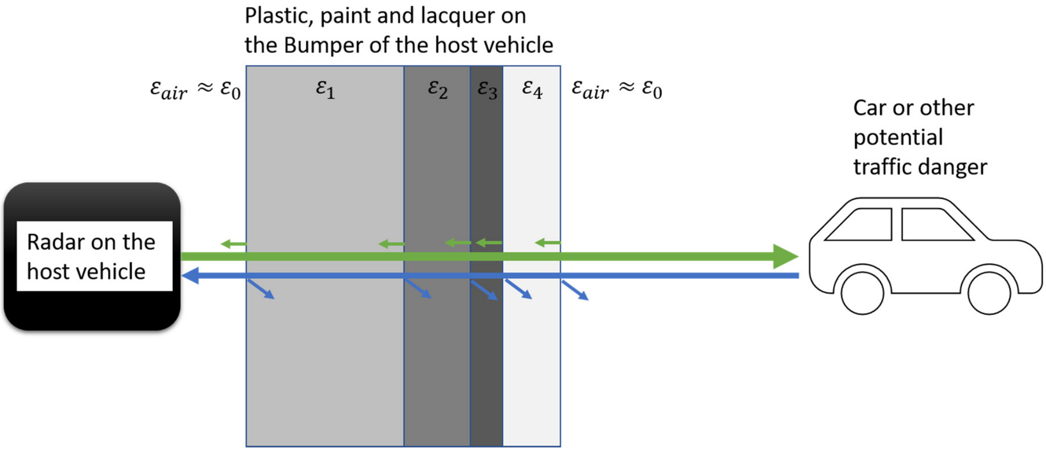

Figure 3: Diagram of radar and painted bumper with permittivites and boundaries.

When electromagnetic waves travel between dielectric media with different dielectric constants, there is reflection and refraction. It is a good estimate to approximate the wave as a plane wave traveling through space in one direction (z in this case, with the wave polarized in x):

$$\overrightarrow{\boldsymbol{E}_\imath}(z) = \vec{a}_x E_{i0} e^{-\beta z}$$

where β includes information for the dielectric's permittivity [8]. At a boundary, the incident (i), reflected (r), and transmitted (t) waves must satisfy:

$$\overrightarrow{\boldsymbol{E}_\imath}(z) = \overrightarrow{\boldsymbol{E}_r}(z) + \overrightarrow{\boldsymbol{E}_t}(z)$$

The intrinsic impedance for a material i is written as:

$$Z_i = \sqrt{\frac{\mu_i \mu_0}{\varepsilon_i \varepsilon_0}}$$

where the ε_0 and μ_0 are the permittivity and permeability for free space, respectively. At the boundary, for an incident wave at normal incidence traveling from material 1 to 2, the reflection coefficient is:

$$r = \frac{E_{r0}}{E_{i0}} = \frac{Z_2 - Z_1}{Z_2 + Z_1} = \frac{\sqrt{\frac{\mu_2\mu_0}{\varepsilon_2\varepsilon_0}} - \sqrt{\frac{\mu_1\mu_0}{\varepsilon_1\varepsilon_0}}}{\sqrt{\frac{\mu_2\mu_0}{\varepsilon_2\varepsilon_0}} + \sqrt{\frac{\mu_1\mu_0}{\varepsilon_1\varepsilon_0}}} \approx \frac{\sqrt{\varepsilon_1} - \sqrt{\varepsilon_2}}{\sqrt{\varepsilon_1} + \sqrt{\varepsilon_2}}$$

and the transmission coefficient is

$$t = \frac{E_{t0}}{E_{i0}} = \frac{2Z_2}{Z_2 + Z_1} = \frac{2\sqrt{\frac{\mu_2\mu_0}{\varepsilon_2\varepsilon_0}}}{\sqrt{\frac{\mu_2\mu_0}{\varepsilon_2\varepsilon_0}} + \sqrt{\frac{\mu_1\mu_0}{\varepsilon_1\varepsilon_0}}} = \frac{2\sqrt{\varepsilon_1}}{\sqrt{\varepsilon_1} + \sqrt{\varepsilon_2}}$$

The reflection and transmission coefficients tell how much of an incident wave is reflected and transmitted respectively. They have the following relationship:

$$r + t = 1$$

For radar transparency, one seeks to minimize *r* and maximize *t* for each interface.

2.1.3. Half-wavelength thickness

The wavelength of electromagnetic radiation through a dielectric is dependent on the dielectrics real permittivity. When the thickness of the dielectric is exactly half of the wavelength, incident radiation reflected off both boundaries of the dielectric cancel each other out, as shown in *Figure 4*. More specifically, the condition [5] is:

$$l_i = m\frac{\lambda_i}{2}$$

where l_i is the thickness of dielectric layer i, m is an positive integer, and λ_i is the wavelength of the ith dielectric layer EM radiation in the material. The phenomenon also appears in multi-layered dielectrics, but with the addition of other reflected waves from the other boundaries.

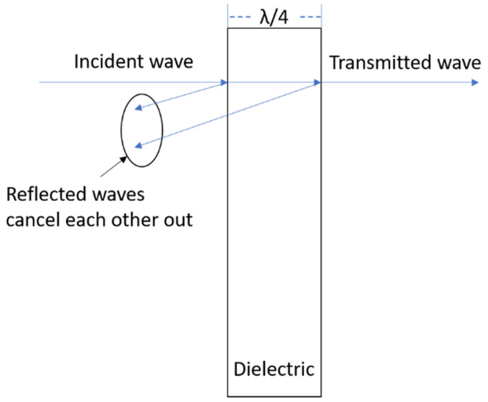

Figure 4: Illustration of quarter wavelength destructive interference of reflected waves from boundaries.

2.2 Polymer and fillers

A large part of the project is spent on the analysis of the materials in the samples. This section will explain the most important characteristics of the materials analyzed.

2.2.1 Polypropylene

Polypropylene (PP) is the plastic in the substrates that most samples will contain. The monomer units are propylene molecules, which are polymerized into long chains. Isotactic PP has monomers stereochemical configuration in the same direction, while atactic has no regular configuration [11]. The former is the more often produced due to its preferred due to its better mechanical and thermal properties.

PP can be a homopolymer, meaning it's mainly PP monomers. It can also be a copolymer meaning it is a mixture of PP and ethylene in lesser amounts.

Pure PP will take longer to crystallize when cooling than PP that has nucleating agents. Nucleating agents provide sites where the chains can begin to form crystals in the form of spherulites. There are both α and β phases for the spherulites, which correspond to two types of crystallographic structure.

PP will crystallize to different percent crystallinity depending on the temperature and speed at which it is crystallized [12]. The amount of each phase, α-PP or β-PP, can be controlled with the cooling temperature [13] [14] [15] and different types of nucleating agents [16] [17]. Carbon black, a common filler in PP-blends, can in lesser amounts promote polymer crystallinity. In substantial amounts it can also inhibit it [18]. Similarly, talc, another common filler in PP-blends, can also promote crystallinity in smaller amounts and inhibit it in larger amounts [19]. Because of these dependencies, it is also possible to control the level of crystallinity by changing the cooling rate, cooling temperature and nucleating agents. For the same reasons, when the molding temperature is not homogeneous, inconsistencies can form in the substrate. An example of this is in during molding when the outer layer is exposed to cooler temperatures than the bulk [20].

2.2.2. Metal flakes

Some of the samples being tested will have metal flakes in the basecoat to create an visual effect. Adding metal particles to a dielectric will change its properties, as the basecoat will no longer be a homogeneous dielectric. At high concentration of metal flakes, a percolation threshold will be reached. In this region, the composite material will have the electromagnetic properties of a metal [21]. This happens when the flakes are connected in a network in the non-conductive bulk.

The higher the frequency of electromagnetic radiation hitting a conductor, the more important the skin effect becomes. Metal flakes have large surface are to volume ration, but at microwave frequencies electromagnetic radiation will not penetrate the entire metal if too thick. Since there are many geometries and sizes of metal particles that are called metal flakes, it is important to take into consideration the skin effect when comparing them to their radar transparency.

Models exist that attempt to estimate the permittivity of a dielectric with conducting particles, such as metal flakes. Maxwell/Wagner/Sillars Polarization [22] is a such a model, but it requires the permittivity of both the dielectric and conductor to be known. Additionally, it estimates the particles as spheres and for them to be evenly distributed, which is not the case for metal flakes. Nevertheless, the model, which will not be further discussed in this thesis, is of relevance to composites such as the basecoat.

3 Materials and Method

The experiments were done on a total of 25 different configuration of polymer blends, primers, basecoats and clearcoats. Two plates of each configuration (except for sample 19), were analyzed. The experiments can be divided into four parts:

1. Radar measurements (dielectric spectroscopy) using the free-space method
2. Thickness measurements using optical microscope
3. Compositional and structural analysis using optical microscope, SEM/EDX, TGA, DSC, and FT-IR
4. Modeling in MATLAB

The following diagram shows a general outline of the procedure:

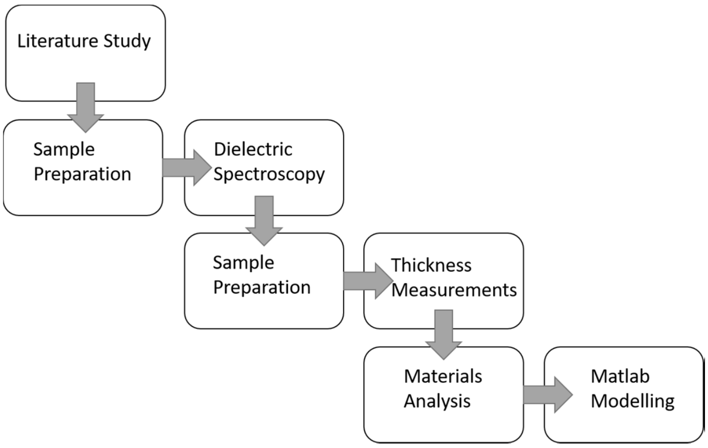

Figure 5: Diagram of the project's method

Not all the methods attempted will be discussed in detail in this report:

The waveguide method [23] for dielectric spectroscopy was to be done on the plastic substrates. In theory, it is a more accurate permittivity measurement than the free space method, as there are virtually no electromagnetic losses to the outside of the waveguide. However, the uncertainties are much greater due to the small sample dimensions that could mean small irregularities in the cut pieces have a relatively large impact on measurement. Since the experiments are done on plastics, cutting could also change a relatively large part of the bulk structure, as polymers are more heat sensitive than metals. Since there were difficulties in cutting the plastic samples into the correct sizes (3,1x1,5 mm), the waveguide method was unfortunately not done on the samples in this study, but due to the uncertainties in using plastic with the wave-guide method, the free-space method was more reliable in the end.

Some samples were also cut and sent to other companies for similar dielectric spectroscopy analyses. Unfortunately, the measurements were not received in time for comparison against our measurements.

Ultrasound measurements were also performed on all the sample coatings using a device that measures coating thicknesses with ultrasound. However, the speed of sound through each layer was required for accurate measurements and the signals were not clear for all the layers due to similar acoustic impedances for adjacent layers. Additionally, errors for basecoat thicknesses varied from 0.6% to 26%, rendering it unviable for permittivity calculations that relies on accurate thickness measurements.

Initially, cutting with a microtome was to be done on the samples for coating thickness measurements. However, after many failed attempts, the samples were cut, placed in epoxy, sanded and polished instead.

3.1. Samples

Table 1: Matrix for all the sample configurations used in the study.

Sample	Plastic substrate	Primer	Base Coat 1	Top Coat 1	Base Coat 2	Top Coat 2	Base Coat 3	Top Coat 3
S1	PP_1	-	-	-	-	-	-	-
S2	PP_2	-	-	-	-	-	-	-
S3	PP_3	-	-	-	-	-	-	-
S4	PP_4	-	-	-	-	-	-	-
S5	PP_5	-	-	-	-	-	-	-
S6	PP_6	-	-	-	-	-	-	-
S7	PP_7	-	-	-	-	-	-	-
S8	PP_8	-	-	-	-	-	-	-
S9	PP_8	Pr_1	-	-	-	-	-	-
S10	PP_8	Pr_1	BC_1	-	-	-	-	-
S11	PP_8	Pr_1	BC_1	CC_1	-	-	-	-
S12	PP_8	Pr_1	BC_1	CC_1	BC_1	CC_1	-	-
S13	PP_8	Pr_1	BC_2	CC_1	-	-	-	-

S14	PP$_8$	Pr$_1$	BC$_3$	CC$_1$	-	-	-	-
S15	PP$_8$	Pr$_1$	BC$_4$	CC$_1$	-	-	-	-
S16	PP$_8$	Pr$_1$	BC$_5$	CC$_2$	-	-	-	-
S17	PP$_8$	Pr$_1$	BC$_6$	CC$_1$	-	-	-	-
S18	PP$_8$	Pr$_3$	BC$_{7.1}$	CC$_1$	-	-	-	-
S19	PP$_{10}$	Pr$_4$	BC$_8$	CC$_4$	-	-	-	-
S20	PP$_3$	Pr$_1$	BC$_1$	CC$_1$	BC$_9$	CC$_3$	-	-
S21	PP$_3$	Pr$_1$	BC$_1$	CC$_1$	BC$_9$	CC$_3$	BC$_9$	CC$_3$
S22	PP$_3$	Pr$_1$	BC$_3$	CC$_1$	BC$_{10}$	CC$_3$	-	-
S23	PP$_3$	Pr$_1$	BC$_3$	CC$_1$	BC$_{10}$	CC$_3$	BC$_{10}$	CC$_3$
S24	PP$_9$	-	-	-	-	-	-	-
S25	PP$_3$	Pr$_2$	-	-	-	-	-	-
S26	PP$_3$	Pr$_2$	-	CC$_1$	-	-	-	-

25 sample configurations were studied. The plastics company was kind enough to supply S1, S3-19, and S24-26. Some of the samples mimic factory produced bumpers on automobiles. S2 never arrived, so it is not part of the study. S20-S24 were samples that were repainted at Volvo Cars to mimic bumpers that have been repainted for aftermarket purposes. S20 and S22 have one layer of aftermarket basecoat and topcoat. S21 and S23 have two layers of basecoat and topcoat.

Before the radar measurements, the samples were cleaned. Before the thickness measurements, the samples were first cut with a bandsaw, then smaller pieces were cut with a water-cooled diamond saw. The samples were placed together into four separate blocks and cured in epoxy. Afterwards the blocks were sanded and polished until they were ready to be looked at under microscope.

3.2. Dielectric spectroscopy – Free space method

There are several methods to measure the dielectric constant in a material. This thesis project used the horn antenna method. The benefits of this method is that it doesn’t require any cutting of the samples, and it is relatively fast to do many samples within a short time. For the thesis, the radar measurements were done in conjunction with another company specializing in signals processing.

For the horn antenna method, we placed the plate in-between two transmitter/receivers in air. All 25 samples were done using this measurement method at the frequency range of 60-90GHz.

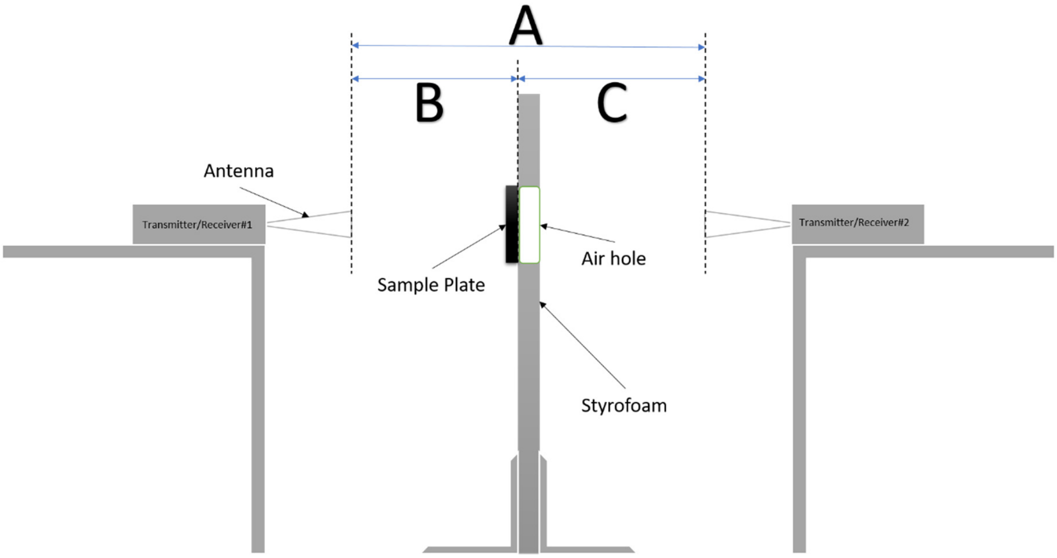

Figure 6: Diagram of the free-space method setup. The styrofoam is used to hold the sample, and a hole is cut where the sample sits above to minimize interference. A, B, and C are the distance between the antennas, and the distances two the sample surfaces from the transmitters/receivers, respectively.

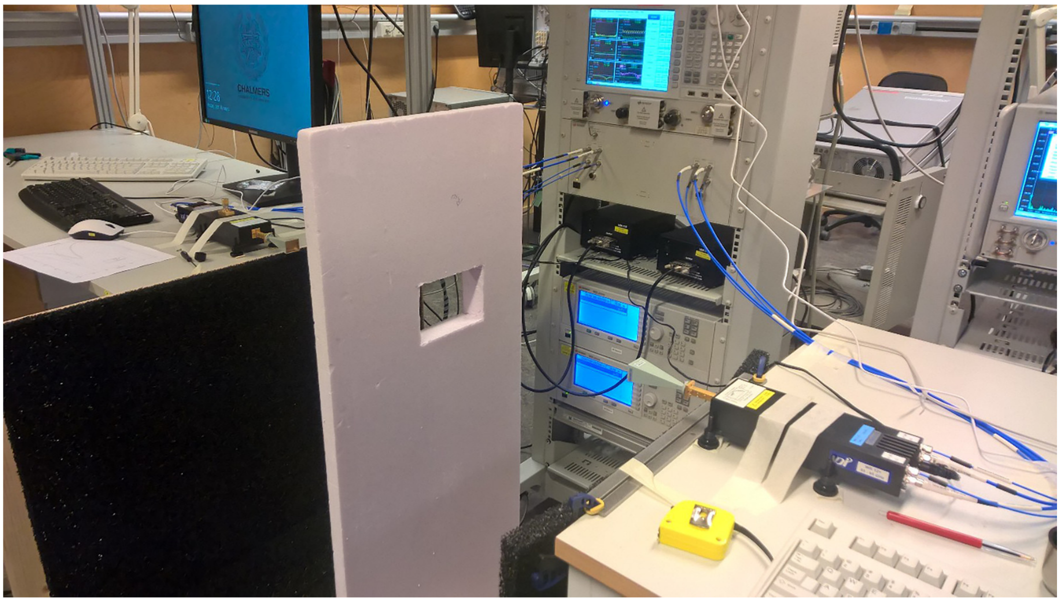

Figure 7: Picture of the free-space method setup performed at Chalmers MC2.

3.2.1. Measurements and data from the free-space method: S-parameters

The data from the free-space method is measured on a network analyzer. Signals from one transmitter/receiver is sent out and measured on both between 60-90GHz. Then signals from the other is sent out and measured on both. We are left with 4 measurements, also known as the scattering parameters (S-parameters): S_{11}, S_{12}, S_{21}, and S_{22}. *Figure 8* illustrates how the scattering parameters work. Only the S_{11} and S_{21} parameters were needed, due to redundancies.

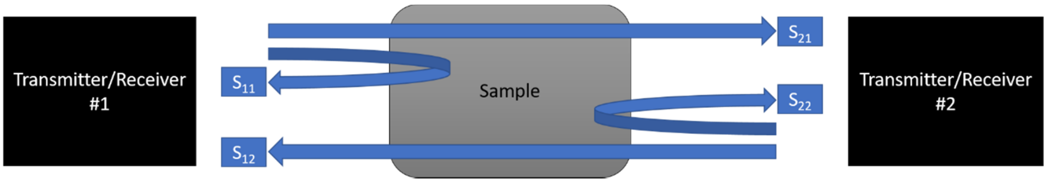

Figure 8: 2-port junction [24].

To cancel unwanted reflections from the Styrofoam, time-domain gating is done [25]. To relate the S-parameters to the reflection and transmission coefficients, normalization measurements and calculations must be done on the measured S-parameters. An empty measurement with just the Styrofoam is done to later divide measurements for normalization of S_{21} measurement by:

$$S_{21}^{norm} = \frac{S_{21}}{S_{21}^{empty}}$$

where S_{21}^{empty} is the measurement done with the empty Styrofoam, S_{21} is the measurement done with the sample, and S_{21}^{norm} is the normalized measurement, equal to the transmission coefficient t for all layers combined. Similarly, for S_{11} and S_{22}

$$S_{11}^{norm} = \frac{S_{11}}{S_{11}^{metal}}$$

where S_{11}^{metal} is a measurement done with a reflective metal plate the same size of the sample, S_{11} is the sample measurement, and S_{11}^{norm} is the normalized measurement equal to the reflection coefficient r for all layers combined.

3.2.1. Measurements and data from the horn antenna method: multilayer dielectrics

Pfeiffer and Biebl [6] outline a method of finding the reflection coefficient, *r*, and transmission coefficient, *t*, of a multilayered structure in air, like the painted car bumper. It is of our interest in this study to discover the materials that minimize *r* and maximize *t*. In our measurements we assume that the bumper is flat, the waves are planar, and the incident waves are normal to the bumper. The dielectric constant, $\varepsilon_{r,i}$, for each layer, starting from the material closest to the bumper, is known. In the article, using transmission line theory, the following equations for *r* and *t* are derived

$$r = \frac{A + B\frac{1}{Z_{w,0}} - CZ_{w,0} - D}{A + B\frac{1}{Z_{w,0}} + CZ_{w,0} - D} = S_{11}^{norm}$$

$$t = \frac{2}{A + B\frac{1}{Z_{w,0}} + CZ_{w,0} - D} = S_{21}^{norm}$$

where the letter values are derived from the matrix

$$\begin{pmatrix} A & B \\ C & D \end{pmatrix} = \prod_{i=1}^{N} \begin{pmatrix} \cos\varphi_i & jZ_{w,0}\sin\varphi_i \\ j\frac{1}{Z_{w,0}}\sin\varphi_i & \cos\varphi_i \end{pmatrix}$$

and the line impedance for E- and H-polarization respectively in the *i*th material from the radar are

$$Z_{w,i}^{E} = Z_0 \frac{\cos\theta_i}{\sqrt{\varepsilon_{r,i}}}$$

$$Z_{w,i}^{H} = \cos\theta_i \sqrt{\varepsilon_{r,i}}$$

where the impedance of free space, $Z_0 = \sqrt{\frac{\mu_0^2}{\varepsilon_0^2}} = 377\Omega$. Finally, the phase difference, φ_i, is:

$$\varphi_i = d_i \frac{2\pi}{\lambda_0} \sqrt{\varepsilon_{r,i}} \cos\theta_i,$$

where d_i is the thickness of the *i*th material, λ_0 is the free space wavelength, $\varepsilon_{r,i}$ is the dielectric constant of the *i*th material, and θ_i is the angle of incidence into the *i*th material.

The only unknown parameters in the samples are the permittivities of the materials and the thickness of the layers. After the measurements in the optical microscopes, only the permittivities are left. One can only find the permittivity of one layer at a time, as there will be too many unknown parameters if one tries to do more at once. In the sample matrix, S8-S10 have the same substrate and primer as most of the other samples. By measuring each, one can find the dielectric constant of almost all the layers from our sample matrix using this method.

3.3. Thickness measurement and sample observation with optical microscope and SEM

After the samples have been cut, put into an epoxy block, sanded and polished, thickness measurements and sample evaluation of the samples in optical microscope could be done. Each layer was measured three times and an average of the three was used to calculate the dielectric constant from the free-space measurements.

The Scanning Electron Microscope (SEM) analysis was done with both secondary electron (SE) and backscattered electron (BSE) modes. SE electrons provides topographical information about the sample and BSE provides contrast between atoms with high difference in atomic number. Although the surfaces were flat, the use of the SE mode was sometimes useful. The samples were carbon sputtered before the analysis in order to eliminate charge buildup. The samples were observed at high vacuum.

Both microscope and SEM images were taken to observe the plastic, the coatings and the effect pigments.

3.4. Material analysis with TGA, DSC, FT-IR, and EDX

After determining the dielectric constant, materials analysis on samples that required further information on the composition.

3.4.1. FT-IR

Fourier Transform Infrared (FT-IR) Spectroscopy was performed on a Thermo Scientific Nicolet iS50 FT-IR that measured the absorbance spectrum. FT-IR determines the functional groups in a material, and it is therefore useful at identifying compounds with several types of covalent bonds. FTIR only penetrates 5-10μm, meaning that it is suitable for analysis of coatings [26]. Unfortunately, almost all our samples had a clearcoat, so only measurements on the plastics were useful.

3.4.2. TGA

Thermogravimetric Analysis (TGA) heats a small piece of a sample up to a temperature that evaporates and combusts it, while constantly measuring the weight of the sample. Since different compounds have different boiling and burning temperatures, the amount of polymer matrix, talc, carbon black and other inert materials can be calculated from this analysis.

The program that was run on all the samples was the following:

1. Heat from 50°C to 300°C at 25K/min with 55ml Nitrogen gas/min
2. Stay at 300°C at 25K/min with 55ml Nitrogen gas/min for 10 minutes
3. Heat from 300°C to 800°C at 25K/min with 55ml Nitrogen gas/min
4. Stay at 800°C at 25K/min with 55ml Oxygen gas/min for 20 minutes
5. Heat from 800°C to 900°C at 25K/min with 55ml Oxygen gas/min

The TGA used was a Mettler Toledo TGA/DSC 1 STAR e System and analysis was done with Omnic software.

3.4.3. DSC

Differential Scanning Calorimetry (DSC) was used to determine the glass transition temperature and calculate the degree of crystallinity in the plastic samples. It works by heating up the sample with at a constant temperature rate, and measuring the heat flux. Around the melting temperature, the sample requires more energy to increase in temperature.

DSC can be to calculate the degree of crystallinity for a plastic sample. The PP blends have spherulites that are crystalline that require heat to melt. A plastic is never 100% crystal, but through extrapolation, a value for the enthalpy of melting such a crystal, ΔH_0, exists in as a reference value. For pure isotactic PP it's 207.1 J/g [27]. By taking the integral of the DSC heat curve, the melting enthalpy, ΔH_m, can be obtained. To determine the crystallinity of our samples the following relation was used:

$$X_c(\%) = \frac{\Delta H_m}{\Delta H_0} \times 100$$

The assumption required to use this equation is that we have pure PP. We use FT-IR results to see if this assumption is true. TGA analysis is also required to find the actual ΔH_m for samples that have fillers in them, as the fillers do not melt when the plastic spherulites melt. As an additional measure to see if the polymer matrices are mostly PP, the T_m values can be compared to the value for pure PP, and to each other.

The DSC used was a PerkinElmer Instruments Pyris 1 DSC, with nitrogen as the purge gas.

4 Results

4.1 Thickness measurements

Thickness measurements of the plastic samples (1, 3-8 ,24) were done using an electronic caliper at 5 positions. Thereafter an average was taken, as shown in *Table **2***. The standard deviation was taken for the error bars, shown in *Figure **9***. The same method was used to measure the plastic substrate thickness on all the other samples, as the coating thicknesses are relatively minor compared to the substrate thicknesses. To measure the thickness of the coatings, 3 measurements for each layer in each plate were averaged on the cross-sections of each plate using an optical microscope. The primer layer was difficult to see, and was therefore set to the standard 4 mu, which is the information from the supplier.

Table 2: Measured plastic thicknesses for plastic samples

Sample	Plastic Thickness [mm]	
	1	2
S1	3,562	3,584
S3	3,414	3,42
S4	3,544	3,522
S5	3,468	3,474
S6	3,512	3,508
S7	3,488	3,486
S8	3,416	3,446
S24	3,492	3,492

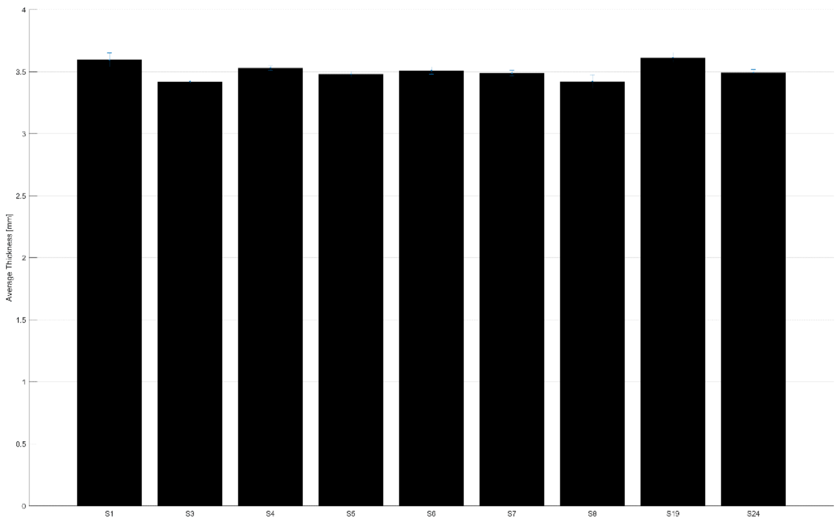

Figure 9: Average plastic sample thicknesses with error bars set at one standard deviation, measured with optical microscope.

4.2 Plastic substrates Material Analysis

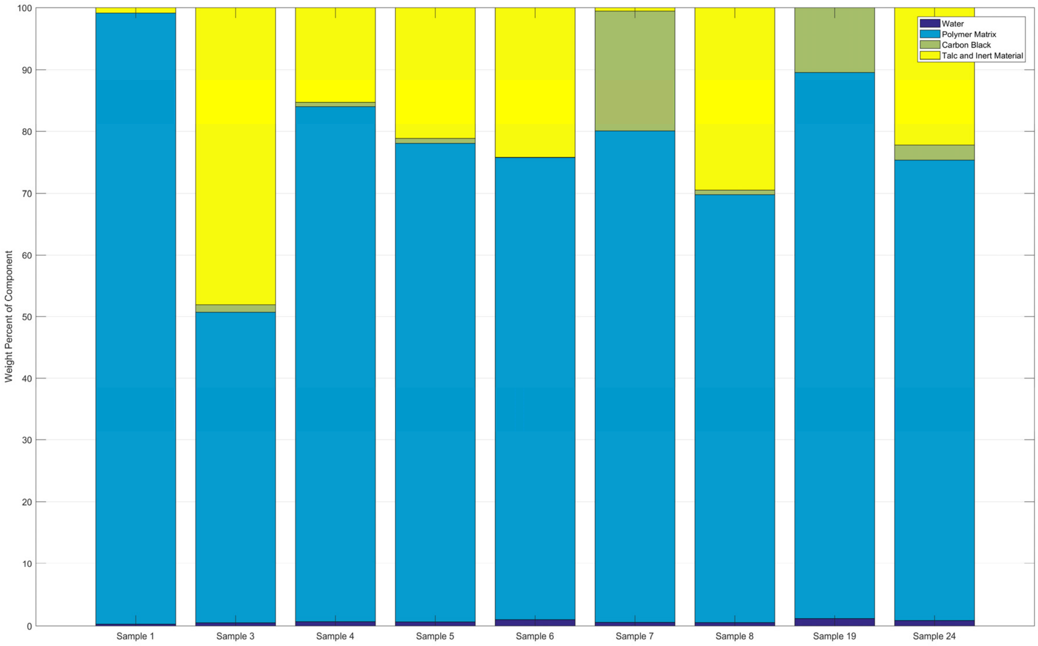

Figure 10: Averages of component concentrations for each sample configuration from TGA results.

Figure 10 shows the compositions of the sample substrates. S1 has some talc or inert material though it's supposed to be pure PP according to the supplier. S7 has substantial amounts of carbon, likely for its radar absorbing ability. S19 also has high concentration of carbon compounds. The other samples have different amounts of talc.

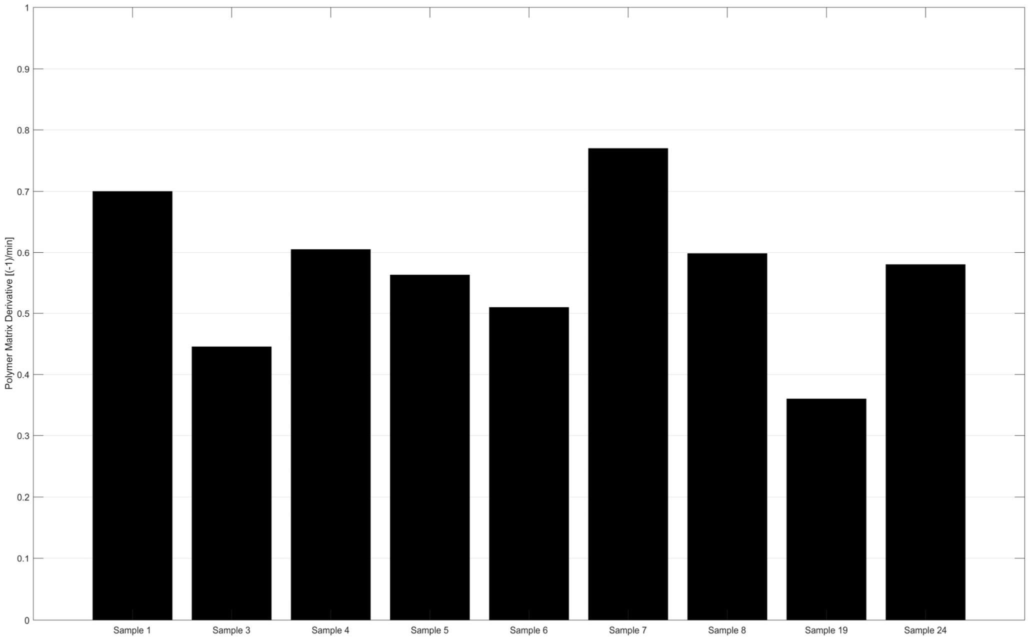

Figure 11: TGA average derivatives for the polymer matrix region. A higher value correlates to a mixture of polymers and bonds that are more alike.

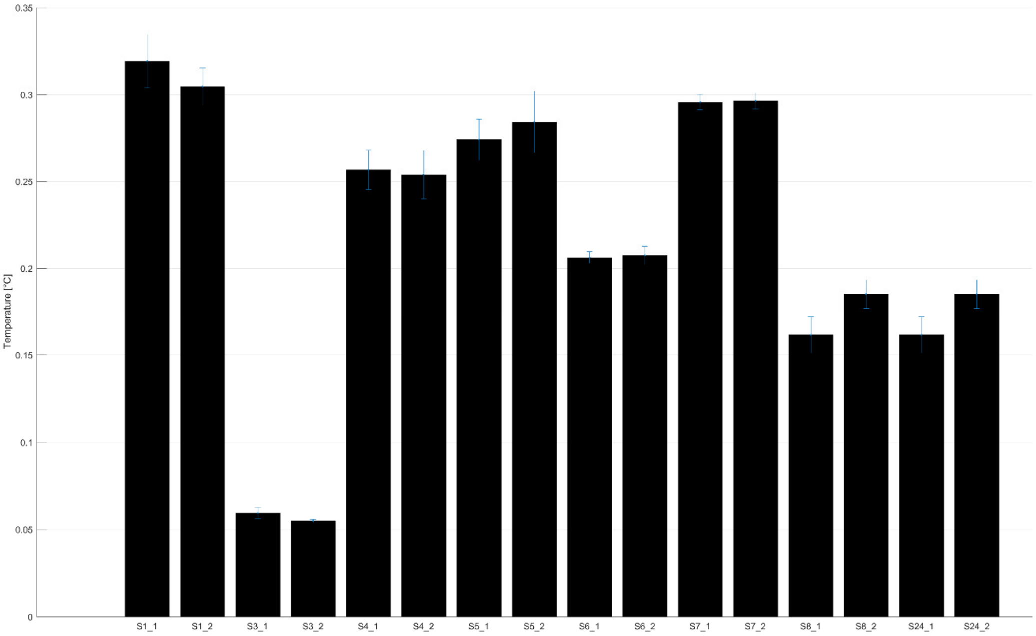

Figure 12: DSC crystallinity for all samples, corrected for filler concentration. H_0 for 100% crystallinity PP was found from a reference to be 207.1 J/g. Error bars at one standard deviation.

S1 has the highest crystallinity, although it also has the least amount of fillers, that can act as nucleating agents. S3 has low crystallinity, likely due to its high talc content which impedes the forming of large spherulites. The rest of the samples have varying crystallinity, but further analysis is required to understand why.

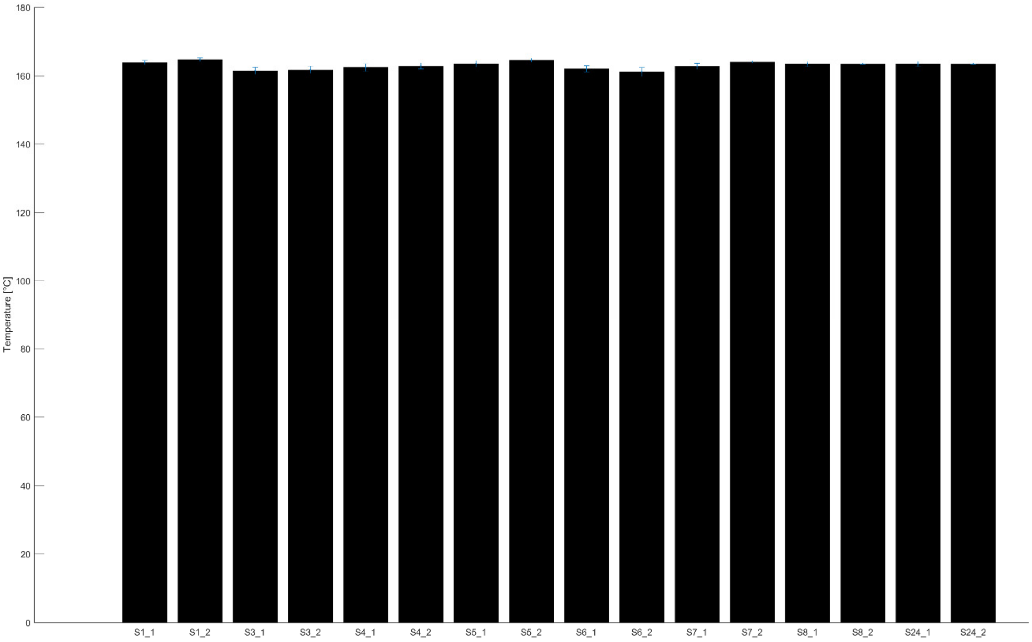

Figure 13: DSC melting temperature, T_m, for all samples. No obvious correlation is apparent.

Table 3: FT-IR First and second highest matching spectra from database for the plastic substrates.

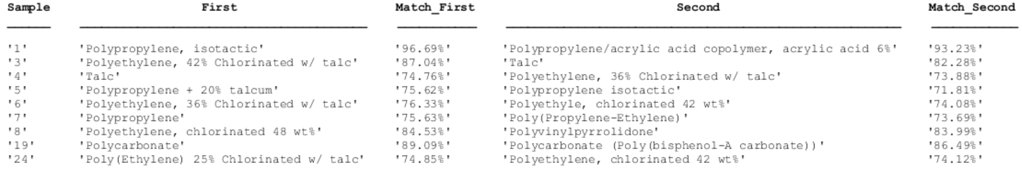

```
Sample                First                      Match_First                     Second                          Match_Second
______    ______________________________________   ___________   _________________________________________________   ____________

'1'       'Polypropylene, isotactic'               '96.69%'      'Polypropylene/acrylic acid copolymer, acrylic acid 6%'   '93.23%'
'3'       'Polyethylene, 42% Chlorinated w/ talc'  '87.04%'      'Talc'                                              '82.28%'
'4'       'Talc'                                   '74.76%'      'Polyethylene, 36% Chlorinated w/ talc'             '73.88%'
'5'       'Polypropylene + 20% talcum'             '75.62%'      'Polypropylene isotactic'                           '71.81%'
'6'       'Polyethylene, 36% Chlorinated w/ talc'  '76.33%'      'Polyethyle, chlorinated 42 wt%'                    '74.08%'
'7'       'Polypropylene'                          '75.63%'      'Poly(Propylene-Ethylene)'                          '73.69%'
'8'       'Polyethylene, chlorinated 48 wt%'       '84.53%'      'Polyvinylpyrrolidone'                              '83.99%'
'19'      'Polycarbonate'                          '89.09%'      'Polycarbonate (Poly(bisphenol-A carbonate))'       '86.49%'
'24'      'Poly(Ethylene) 25% Chlorinated w/ talc' '74.85%'      'Polyethylene, chlorinated 42 wt%'                  '74.12%'
```

FT-IR spectra database matchings, *Table **3***, shows a high likelihood that the polymer matrix for many of the samples is a mixture of PP, polyethylene, acrylic acid, and a chlorine compound. S19 is polycarbonate, which explains why it wasn't possible to do DSC measurements on it.

4.3 Coatings pictures

4.3.1. Primer

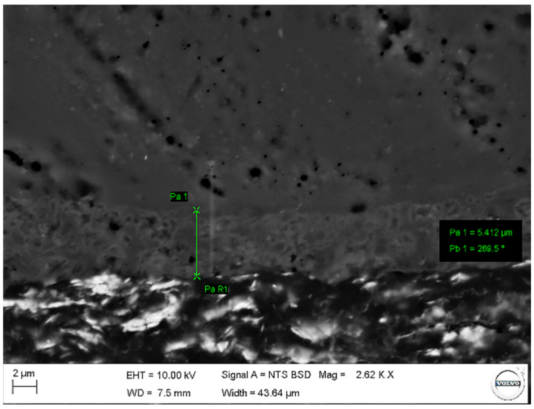

Figure 14: BS SEM image of sample 25 surface at 2620x magnification. The coating is a primer layer with a thickness of 5.4µm.

Although the primer wasn't observable in the optical microscope, later SEM analysis showed that it was possible to measure it with higher magnifications.

4.3.2. Metal Flakes

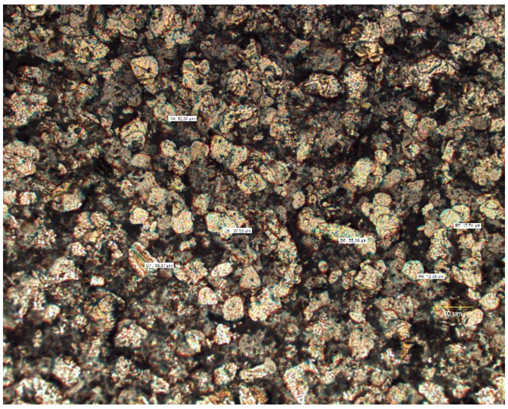

Figure 15: Sample 10 surface at 200x magnification

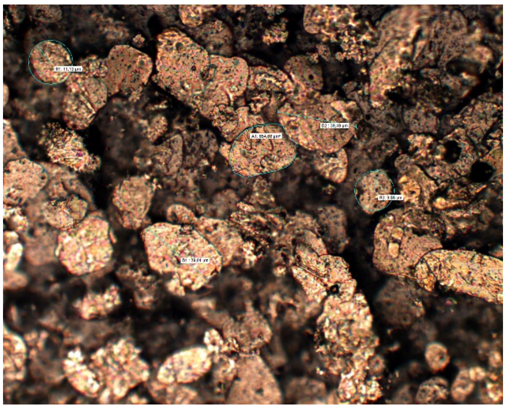

Figure 16: Sample 10 surface at 500x magnification

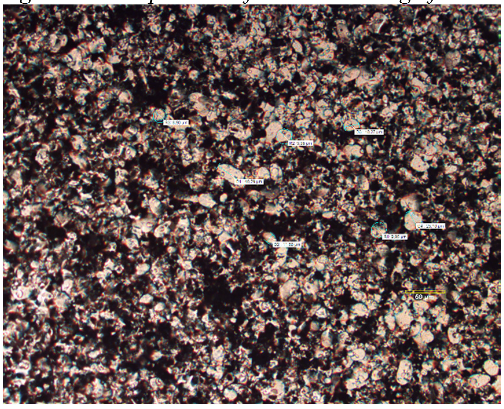

Figure 17: Sample 14 surface at 200x magnification

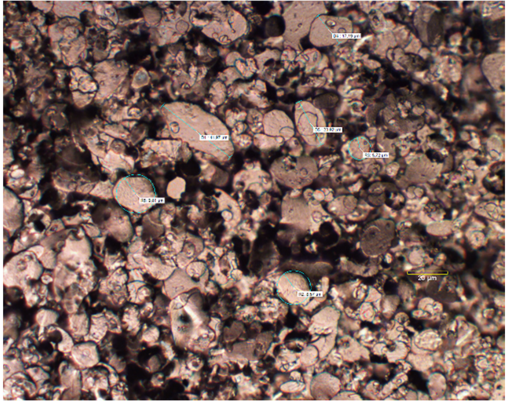

Figure 18: Sample 14 surface at 500x magnification

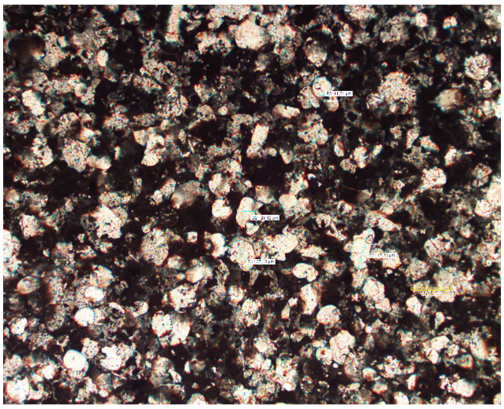

Figure 19: Sample 20 surface at 200x magnification

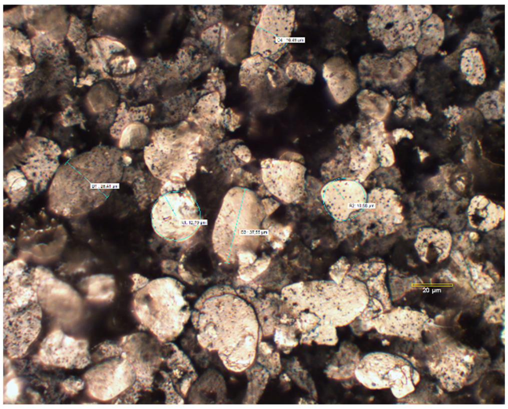

Figure 20: Sample 20 surface at 500x magnification

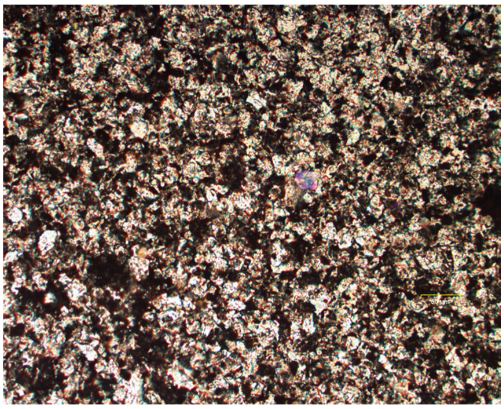

Figure 21: Sample 23 surface at 200x magnification

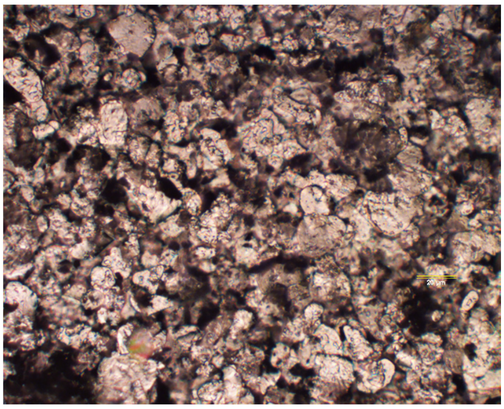

Figure 22: Sample 23 surface at 500x magnification

Figure 15 to *Figure 22* above are show comparisons of four unique basecoat layers with metal flakes. The shapes and sizes are different. Sample 20 shows the aftermarket equivalent of sample 10, and sample 23 shows the aftermarket equivalent of sample 14. Observe that the flakes are larger for samples 10 and 20 than they are for samples 14 and 23.

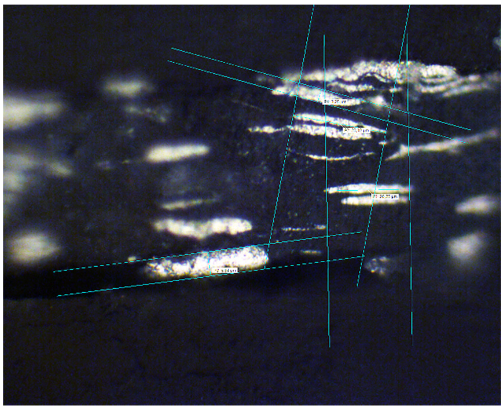

Figure 23: Sample 10 cross-section at 1000x magnification

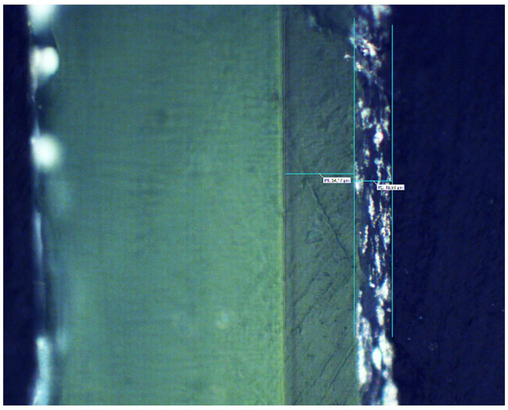

Figure 24: Sample 14 cross-section at 500x magnification

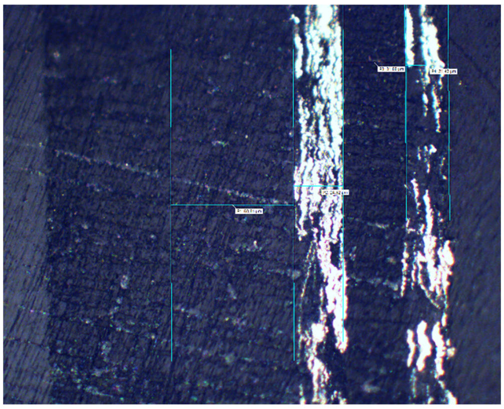

Figure 25: Sample 20 cross-section at 500x magnification. The layer on the left is the aftermarket basecoat.

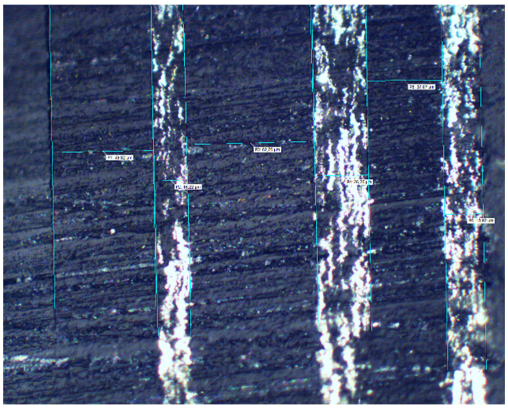

Figure 26: Sample 23 cross-section at 500x magnification. The two layers on the left are the aftermarket basecoats.

Figure 23 to *Figure 26* above show the cross-sections of samples with unique basecoats containing metal flakes. Note that the flakes are generally parallel to the substrate and form clusters.

4.3.3. Other effect pigments

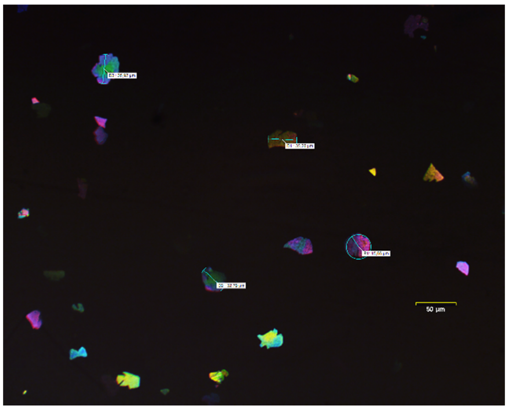

Figure 27: Sample 15 surface at 200x magnification

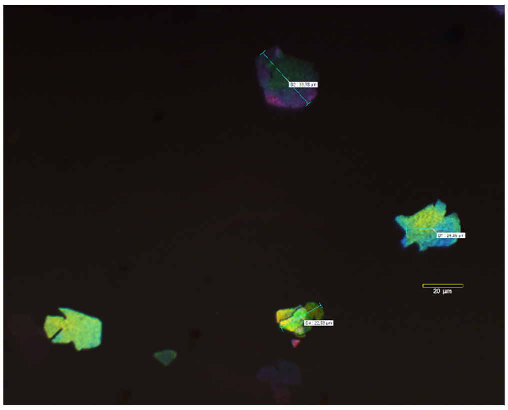

Figure 28: Sample 15 surface at 500x magnification

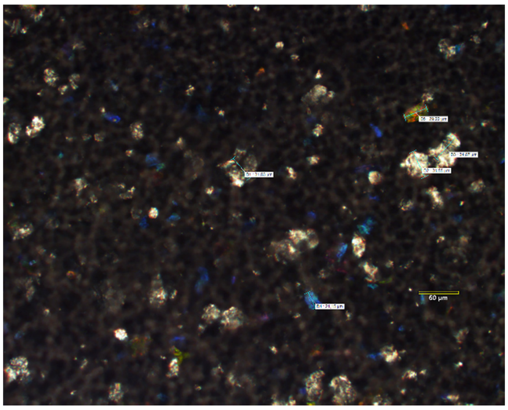

Figure 29: Sample 16 surface at 200x magnification

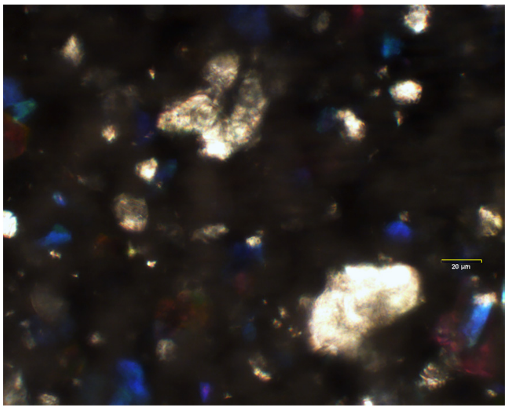

Figure 30: Sample 16 surface at 500x magnification

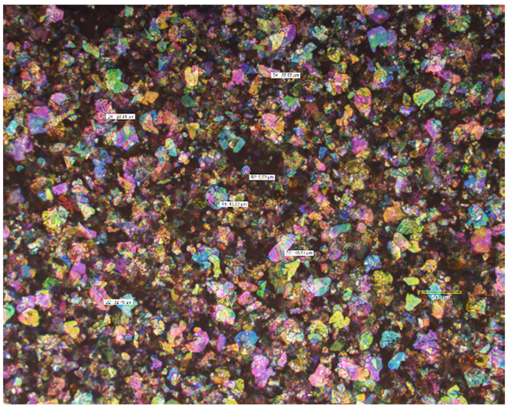

Figure 31: Sample 18 surface at 200x magnification

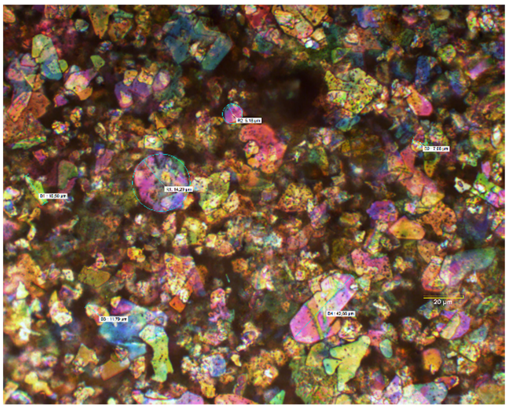

Figure 32: Sample 18 surface at 500x magnification

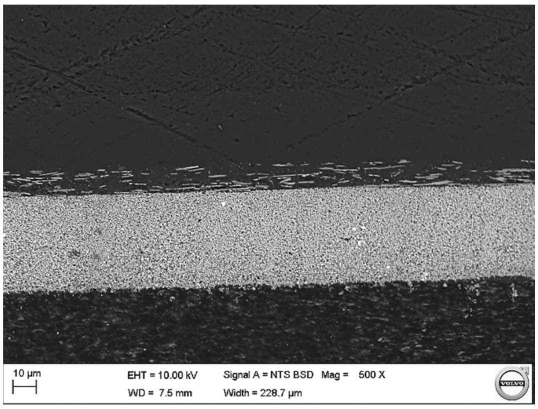

Figure 33: BS SEM image cross-section of sample 18 at 500x magnification

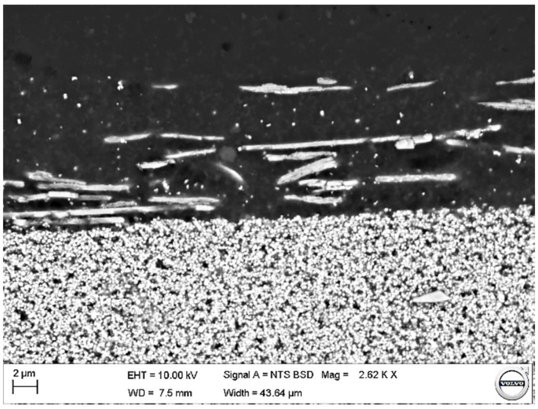

Figure 34: BS SEM image cross-section of sample 18 at 2620x magnification

Figure 27 to *Figure 34* show the microscope and SEM images of the effect pigments. Sample 15 has a low quantity of fillers in the microscope pictures, which is in agreement with the information given by the suppliers. Sample 18 has a high concentration, with some metal flakes lying parallel to the substrate surface, as shown in the SEM images.

4.3.4. PVD coating material analysis

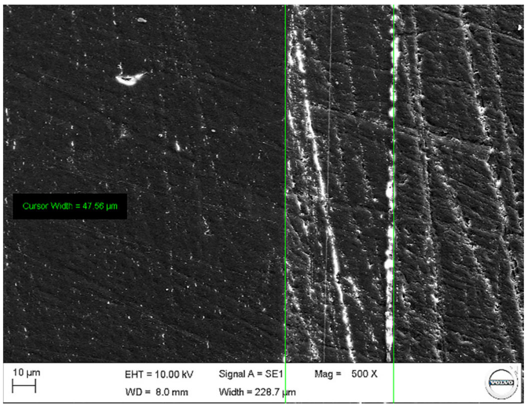

Figure 35: SE SEM image cross-section of Sample 19 at 500x magnification

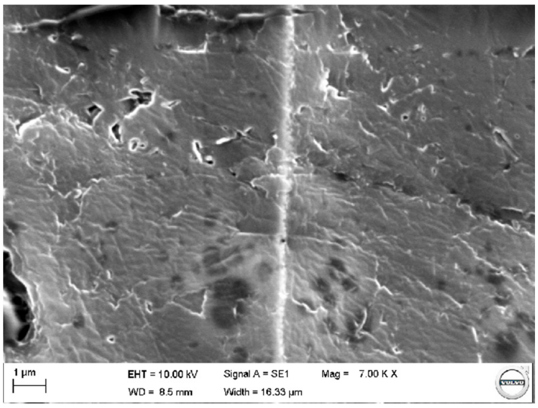

Figure 36: SE SEM image cross-section of Sample 19 coating at 7000x magnification

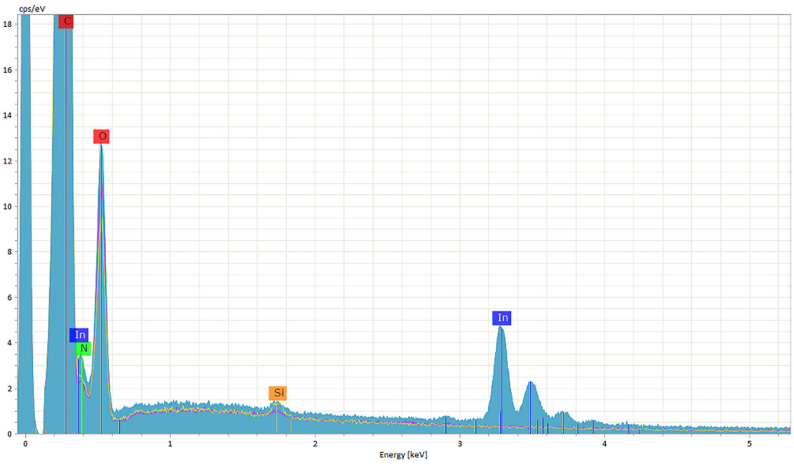

Figure 37: XRD point analysis on sample 19 cross-section PVD coating. SEM and EDX analysis shows a thin layer of indium sandwiched between two layers on the surface of S19.

Figure 35 to *Figure 37* show the SEM images and EDX analysis of the PVD-coated surface of S19. The surface appears to be deposited indium sandwiched between a primer and top coat.

4.4. *Radar analysis*

4.4.1. S parameters

Table 4 summarizes the results of sample measurements and permittivity estimations. The columns 2 and 3 are the resonance frequency, or the frequency at which there is a minimum of reflection for two plates of the same sample configuration. Columns 4 to 9 show the root mean square error (RMSE) for curve fittings using measurements from S_{11}, S_{21}, and the mean of S_{11} and S_{21}, respectively. The values highlighted in green are the minimum values (if under 1.5, except for S7) for which the permittivity is calculated. Columns 10-13 show the S-parameters at 77GHz.

The permittivity for S12 was not calculated due to it containing extra layers. Sample 19 also seemed to exhibit extra layers, but under closer inspection it contained a thin metallic layer sandwiched between two other layers. Additionally, no radar measurements had been done on the plastic for S19 prior, so no permittivity could be calculated from this sample. The high number of layers in S20-S23 caused a spread in the resonance peak, making an accurate curve fitting very difficult. S26 showed almost no variation from S25, so no permittivity measurements were done on this sample either.

Table 4: S parameters for all measured samples.

Sample	Resonance freq. for $\lvert S_{11}\rvert$ (GHz)		Mean RMSE with S_{11} inversion (dB)		Mean RMSE with S_{21} inversion (dB)		Mean RMSE with iterative (dB)		@77 GHz			
									$\lvert S_{11}\rvert$ dB		$\lvert S_{21}\rvert$ dB	
	1	2	1	2	1	2	1	2	1	2	1	2
1	83.8	83.5	**1.12**	**0.77**	1.70	3.98	5.19	6.61	-12.9	-12.9	-0.06	-0.50
3	72.9	72.9	**0.86**	**0.83**	1.04	1.04	2.98	4.13	-11.1	-11.1	-0.40	-0.34
4	79.3	79.2	**0.52**	**0.63**	2.83	2.44	6.57	5.53	-18.1	-18.9	-0.19	-0.01
5	79.8	79.8	**1.26**	**1.22**	3.03	2.40	7.45	5.49	-17.6	-18.2	0.03	-0.30
6	72.0	71.9	**0.77**	**0.56**	0.99	0.54	1.19	1.40	-10.1	-9.78	-0.83	-0.76
7*	-	-	4.34	6.21	**3.13**	**3.27**	6.77	4.84	-5.96	-6.24	-41.2	-36.4
8	77.1	78.6	**0.99**	**1.04**	2.56	1.51	4.45	5.90	-33.0	-21.2	-0.09	-0.08
9	77.7	77.7	**1.29**	**1.17**	2.68	2.64	3.89	3.65	-28.1	-27.1	0.04	0.11
10	71.3	73.2	0.77	**1.40**	**0.69**	2.21	4.95	4.19	-6.59	-7.62	-1.77	-1.25
11	70.4	71.5	**0.62**	**0.94**	0.78	2.12	10.5	12.8	-4.86	-5.75	-2.34	-1.98
12	68.1	67.9	NaN	NaN	NaN	NaN	NaN	NaN	-2.88	-3.18	-5.09	-5.15
13	74.5	74.2	**0.68**	**0.70**	1.20	1.09	1.77	1.20	-17.0	-15.0	-0.28	-0.11
14	71.6	72.5	**1.00**	2.30	1.77	1.80	3.81	1.80	-7.59	-8.87	-1.13	-0.87
15**	76.5	77.3	1.14	2.53	1.35	2.60	**1.14**	3.11	-29.19	-32.57	0.04	0.10
16	75.6	75.3	**0.91**	**0.89**	1.22	2.08	1.39	2.06	-22.12	-20.54	-0.42	-0.34
17	77.5	76.2	2.39	0.94	2.46	1.88	3.21	**0.87**	-29.75	-25.70	0.05	0.05
18	72.2	74.3	**0.92**	1.84	1.33	1.80	2.28	1.79	-9.81	-13.86	-0.47	-0.18
19	74.3	-	NaN	-	NaN	-	NaN	-	-15.85	-	-0.75	-
20	66.3	66.9	NaN	NaN	NaN	NaN	NaN	NaN	-2.00	-1.94	-9.45	-9.16
21	89.2	89.2	NaN	NaN	NaN	NaN	NaN	NaN	-1.78	-2.00	-10.06	-10.03
22	67.9	67.0	NaN	NaN	NaN	NaN	NaN	NaN	-2.89	-2.79	-5.30	-5.91
23	77.0	68.5	NaN	NaN	NaN	NaN	NaN	NaN	-2.35	-2.81	-6.45	-5.85
24	76.7	76.6	**0.90**	**0.93**	2.69	1.94	4.11	4.65	-32.29	-31.42	-0.15	0.01
25	77.2	77.2	**1.19**	**1.07**	1.99	2.37	2.94	3.79	-31.87	-33.45	-0.36	-0.48
26	76.1	75.8	NaN	NaN	NaN	NaN	NaN	NaN	-27.03	-24.12	-0.17	-0.41

4.4.2 Dielectric Constants

Table 5: Calculated complex permittivities for all the plastic substrates, excluding the substrate for sample 19.

Sample	Mean complex permittivity ($\bar{\epsilon_r}$) for optimal inversion	
	1	2
1	2.23-j0.010	2.24-j0.002
3	3.25-j0.009	3.24-j0.016
4	2.58-j0.019	2.58-j0.019
5	2.62-j0.001	2.62-j0.007
6	3.17-j0.016	3.18-j0.018
7*	*7.64-j3.595	*0.01-j3.13
8	2.90-j0.031	2.79-j0.007
24	2.82-j0.018	2.83-j0.017

The permittivity wasn't calculated for sample 19, but other studies show a high imaginary permittivity in polycarbonate [28].

Table 6: Calculated complex permittivities for the primers

Sample	Mean complex permittivity ($\bar{\epsilon_r}$) for optimal inversion	
	1	2
9	2.81-j0.024	2.81-j0.031
25	2.78-j0.036	2.79-j0.029

Table 7: Calculated complex permittivity for the basecoat in sample 10

Sample	Mean complex permittivity ($\bar{\epsilon_r}$) for optimal inversion	
	1	2
10	40.16-j0.000	34.01-j0.000

Calculations for the primer gave non-physical values, but increasing the thickness improved them. However, since the thickness is so small they were omitted in the MATLAB modeling. Omitting the clearcoat gave better fittings (RMSE-values) for most samples. However, in the MATLAB modelling, a value of 3.5 is given for the topcoats, calculated in an article by Schnabel et al. [29].

Table 8: Calculated complex permittivities for basecoats

Sample	Mean complex permittivity ($\bar{\epsilon_r}$) for optimal inversion		Base coat
	1	2	
11	48.94-j0.005	38.45-j0.001	BC1: Effect pigment - 6.24 % Al (SD 24 µm & CF 8-29 µm) |
13	5.99-j1.609	3.04-j1.642	BC2: Solid
14	37.15-j0.002	-	BC3: Effect pigment - 6.41 % Al (SD 4-26 µm)
15	2.978-j0.014	-	BC4: Effect pigment - Xirallic 0,2 % (2-30 µm)
16	7.00-j1.316	9.99-j0.907	BC5: Effect pigment - 0,7 % Al (CF 18-53µm 0,1%, SD 11-32µm 0,5%, SD 4-21µm 0,1%) Mica 5-25µm 0,5%, Mica 5-40µm 0,4%)
17	-	3.22-j0.007	BC6: Solid
18	35.98-j5.576	-	BC7: Effect pigment - No metal content but other unknown effect pigmentation

The trend for the coatings is that the samples with metal flakes and effect pigments have a much greater permittivity than the rest of the samples.

4.4.3. Modeling Repainted samples in MATLAB

S20-S23 are repainted plates that represent aftermarket paint. Due to a less defined resonance peak in the curves with more layers, the RMSE values were too high for permittivity calculated from curve fittings. Instead, a more qualitative approach was done by manually fitting the curves in MATLAB for approximated permittivity values.

MATLAB was used to model the S11 signal in samples S20_1, S21_1, S22_1, and S23_1. S20_1 has one layer basecoat BC1 and one layer BC9, whereas sample S21_1 has one layer basecoat BC1 and two layers BC9. Similarly, sample S22_1 has one layer basecoat BC3 and one layer BC_{10}.

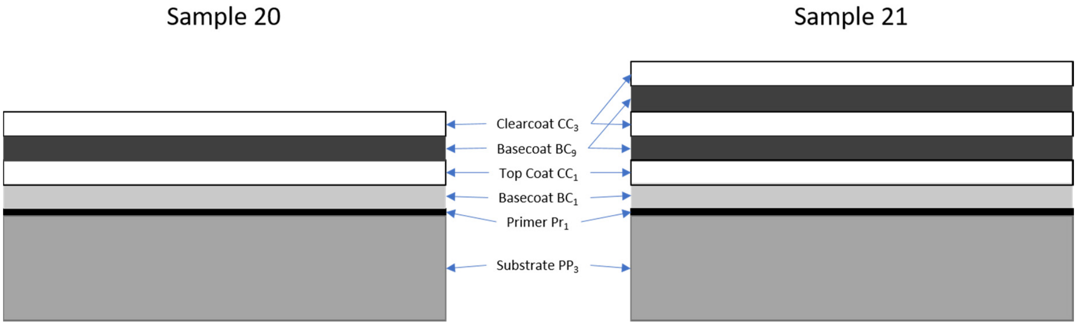

Figure 38: Diagram of samples 20 and 21. The samples have one layer of factory basecoat and topcoat with one or two layers of additional basecoat.

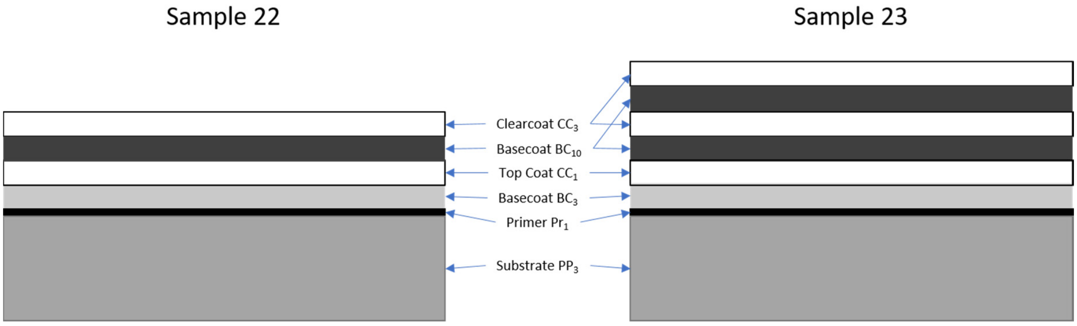

Figure 39: Diagram of samples 22 and 23. The samples have one layer of factory basecoat and topcoat with one or two layers of additional basecoat.

The obtained permittivities for the basecoats repainted with aftermarket paint were around 90-140 for BC_9 in S20 and S21, and 35-70 for BC_{10} in S22 and S23. This was done by matching the minimum reflection and maximum reflections of the modeled curves to the measured S-parameters.

5 Evaluation

5.1 *Metal flakes and effect pigments*

From *Table 8* and *Section 4.4.3.* Modeling Repainted samples in MATLAB, values for permittivities in basecoats with metal flakes and effect pigments can be compared. There is a strong correlation between metal flakes in basecoats and higher real permittivity relative to basecoats that do not have metal flakes or effect pigments. Additionally, although aftermarket repainted samples with metal flakes are, to the untrained eye, visually equivalent to factory basecoats, there is both a higher concentration of metal flakes (*Figure 25* and *Figure 26*) and higher permittivity for the basecoat layer (from the modeling). The difference in number of flakes required is likely due to the difference in method for applying the paint. The factory paints were applied using electrostatic bell method and the aftermarket paints were applied using a conventional spray method. The parameters during painting can affect the metal flakes' orientation, how many flakes are required etc., but a relationship between these and radar transparency are outside the scope of this thesis due to insufficient information from suppliers and insufficient sample variation with metal flakes in the basecoat.

The skin depth for aluminium at 77GHz is calculated to be 0.2955μm from Transmission Lines and Networks [30]. From the microscope pictures, the size and shapes of the metallic flakes seem to be in accordance with the dimensions from the supplier. Since the metal contents of S11 and S13 are about the same, and the flakes are different dimensions it should, in theory, be possible to see a higher permittivity for the smaller flakes due to their relatively larger surface area. However, the radar measurement calculations for the permittivity for S13_1 was between the ones for S11_1 and S11_2. Thus, for our samples no pattern for the size of the metal flakes could be observed.

Under the microscope pictures, there seems to be no large network of connected aluminium particles in any of the samples, so the metal flakes concentration still seems to be below percolation threshold [21]. Thus, the effect of the reason for the permittivity increase for the metal particles is not for this reason in the basecoats.

Samples with other effect pigments also show patterns. S15's basecoat has relatively low permittivity, likely due to the relatively small amount of Xirallic present in the basecoat. S16's basecoat has slightly higher percent effect pigments, and a slightly higher permittivity than S15's basecoat. The low concentrations in these basecoats hints that concentrations at the same levels as metal flakes are not required for the visual effects. Higher concentrations seem too have a greater effect on the radar transparency, but there is not enough data or correlations in this study to make a conclusion on this matter.

S18's basecoat has a real permittivity close to the permittivity for factory basecoats with metal flakes, but no information was given by the supplier about its composition except that it does not contain metal. Also, sample 18 shows higher absorption than any of the other basecoats in our samples. *Figure 34* shows that S18's basecoat contains particles in similar concentrations to other samples with metal flakes in their basecoats. It should from these observations be safe to assume that the effect pigment in S18's basecoat is both conductive and absorptive to 77GHz radar. Further materials analysis of S18's basecoat is of interest as it should definitely be considered in its design in conjunction with radar.

5.2 Polymer fillers and crystallinity

Materials analysis on the polymer substrates showed variations in their polymer matrices, filler concentrations, and crystallinities. From FT-IR analysis, see *Table 3*, all samples substrates except for S19's were a PP-blend of some kind. Most substrates likely contained some polyethylene (PE) and acrylic acid, as well as chlorine. Acrylic acid is likely a nucleating agent as S1's crystallinity was the largest although it had a minimum amount of fillers that could work as nucleating agents [31]. Chlorine was likely present in some samples as residuals from talc production. S19's substrate was polycarbonate from the analysis, but since no radar measurements were done on the substrate itself, no reliable correlations between S19 and dielectric constant could be made.

Figure 12 shows the degree crystallinity for the plastic substrates. The degree of crystallinity was measured for all the sample substrates, except for S19's polycarbonate substrate, which didn't give an enthalpy rise reading in the DSC. Since we couldn't calculate the dielectric constant for S19, the degree of crystallinity was not relevant. For all other sample substrates, 100% crystalline PP was used as a reference to their 100% crystallinity. Although FT-IR analysis showed other components in the polymer matrix, their T_m were very close as shown in *Figure 13*. Had a high percentage of other monomers been present, there would have been another T_m, or a shifted T_m for the melting of the other polymer matrix spherulites.

Figure 10 shows the filler concentrations from TGA analysis. S1 has the lowest amount of fillers and the highest amount of crystallinity, while S3 has the opposite. This difference in crystallinity is likely because the higher number of nucleating agents forms smaller spherulites, and therefore inhibits larger crystalline regions in S3, compared to S1 [31].

Table 5 shows the substrates' calculated permittivities. A comparison to between S1 and S3 can be made to determine talc's effect on radar transparency. The main difference between the samples is the addition of talc in S3. The real permittivity for S1 is the lowest of the substrates and the real permittivity for S3 is the highest. A similar pattern can be found for S4, S5, and S6. It is therefore safe to state that an increase in talc concentration correlates with an increase in real permittivity.

Figure 42 to *Figure 59* in Appendix B shows the SEM images of the plastic substrates. The talc particles seem to favor an orientation parallel to each other in the samples that have a high concentration of talc. There seems to be correlation between the orientation and the permittivity, however the polarization of the S-parameters were also not taken into account in the experimental part of this project. Additionally, too many variables change between the plastic substrates to make a distinction between the orientation of talc and the permittivity of the substrate.

Carbon black, or a similar conducting component, is present in many of the samples. Unfortunately, too many variables changing made it difficult to see a connection between carbon black and radar transparency properly, although the general trend was an increase in imaginary permittivity with an increase in carbon component. Since carbon components are conducting, they concur with the theory [5] that the conduction of a lossy material (a dielectric that is also conductive) is directly proportional to the imaginary permittivity. S7 is designed as a radar absorbing substrate and is likely filled with a carbon-based filler since no compositional contrast was found with BSE SEM analysis (see Appendix B). It is also likely that the filler in S7 has greater conductivity than carbon black, as is common with many radar absorbing composites [32].

5.3 *Optimal thickness and permittivity*

The analyses done in the study revealed the permittivities for most of the substrates and coatings. However, the permittivities themselves only provide limited information as to its influence on radar transparency. Design aspects must also be taken into account. Varying the thicknesses of the substrate and coatings to different values can change the reflected and transmitted signals. Since relatively low imaginary permittivities were discovered for almost all the substrates and permittivities, the focus in increasing radar transparency should be optimizing the thicknesses. Using MATLAB, an example of varying the plastic thickness was done. Focus should be put on changing optimizing the plastic thickness as it has the most impact on the resonance frequency. Additionally, changing the thicknesses of the coatings will affect how the paint looks, meaning that there is less freedom in changing them. Figure 40 shows how one can optimize the thickness of one of the samples when the permittivities and thicknesses are known. By varying the thickness of the substrate, the resonance frequency can be matched to 77GHz [33]. From Figure 40 it can be determined that this optical thickness for minimum reflection is between the red and the yellow curves (close to 3.1mm) for S11_1. The same method can be done for other samples where both the permittivities and thicknesses are known.

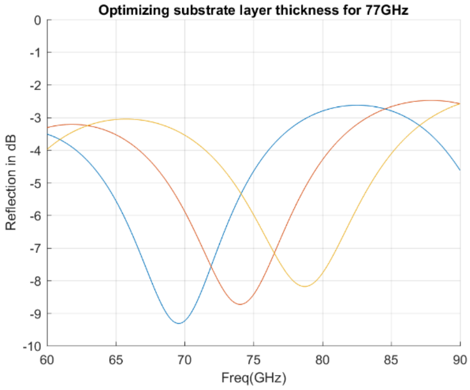

Figure 40: Model in MATLAB of measured S11_1 parameters in blue (3.416mm plastic substrate thickness), slightly thinner substrate thickness in red (3.2mm), and thinner in yellow (3.0mm). Note the different values for each at 77GHz frequency.

Figure 41 shows how an increase in real permittivity can have a negative impact on the resonance peak. Even when matching layers, the real permittivity of the basecoat is a factor that will determine the overall reflection of the bumper.

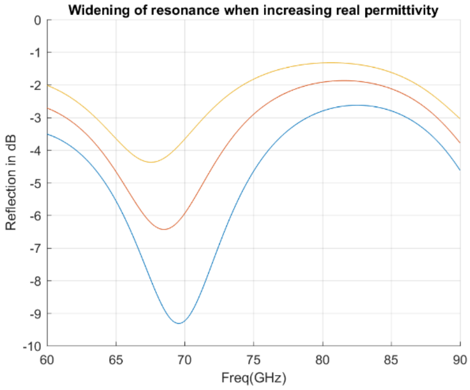

Figure 41: Model in MATLAB of measured S11_1 parameters in blue (real basecoat permittivity = 48.94), higher basecoat permittivity in red (70), and higher in yellow (100). Notice the less defined resonance peak for higher permittivities.

6 Conclusion

25 samples with different configurations of plastic substrate, primer, basecoats and topcoats were analyzed with dielectric spectroscopy at 60-90GHz. Materials analyses of various kinds were done on the samples to identify components and obtain structural information. A strong correlation was observed between for basecoats with high concentrations of effect pigments and higher real permittivity. Higher concentrations of talc in the substrate was also linked to a higher real permittivity.

Modelling in MATLAB showed that the two most important factors in designing a bumper with coatings is to match the thickness of the substrate to the resonance frequency and to minimize the permittivity of the basecoat.

6.1 Considerations for further studies

The question of how concentrations and shapes of effect pigments correlate to radar transparency is left to be answered. A study with more control over the metal flake's variables would be suited for this purpose. The visual appearance of a bumper can be the same for different basecoats containing different shapes and sizes of metal flakes, so perhaps basecoats with the same visual appearance can be studied to find the one with optimal radar transparency. The same type of study can also be performed on other effect pigments.

Finding correlations between plastic substrate percent crystallinity and radar transparency were not found in this thesis due to too many variables changing between the samples. Controlling filler concentration and performing dielectric spectroscopy on samples with different degrees of crystallinity and phases would help in reaching a deeper understanding for how plastics affect radar at 77GHz. Additional analyses, such as X-ray Diffraction (XRD), could also provide extra measures of certainty when analyzing crystallinity.

Finding how the orientation of talc particles affects the dielectrics permittivity can also be interesting. This study made the simplification of the assumption that all materials were isotropic, but SEM images of the talc show a clear pattern in their orientation. This means that the substrates are anisotropic and should have a different permittivity depending on the polarization of the incident radar. Designing the substrates and radars with optimal orientation and polarization could in theory increase the radar transparency without having to change the composition of the substrate.

7. References

[1] J. Hasch, E. Topak, R. Schnabel, T. Zwick, R. Weigel and C. Waldschmidt, "Millimeter-Wave Technology for Automotive Radar Sensors in the 77 GHz Frequency Band," *IEEE Transactions On Microwave Theory And Techniques,* vol. 60, no. 3, pp. 845-860, 2012.

[2] H. H. Meinel, "Evolving Automotive Radar - from the very beginnings into the future," *The 8th European Conference on Antennas and Propogation,* p. 8, 2014.

[3] K.-H. Im, I.-Y. Yang, S.-K. Kim, J.-A. Jung, Y.-T. Cho and Y.-D. Woo, "Terahertz scanning techniques for paint thickness on CFRP composite solid laminates," *Journal of Mechanical Science and Technology,* pp. 4413-4416, 2016.

[4] S. T. d. 93763, Gothenburg, Sweden, 2017.

[5] S. J. Orfandis, "Electromagnetic Waves and Antennas," ECE department, Rutgers University, Piscataway, NJ, 2016.

[6] F. Pfeiffer and E. M. Biebl, "Inductive Compensation of High-Permittivity Coatings on Automobile Long-Range Radar Radomes," *IEE Transactions on Microwave Theory and Techniques,* pp. 2627-2632, November 2009.

[7] J. R. Isasi, L. Mendelkern, M. J. Galante and R. G. Alamo, "The Degree of Crystallinity of Monoclinic Isotactic Poly(propylene)," pp. 323-334, 1998.

[8] D. K. Cheng, Fundamentals of Engineering Electromagnetics, Addison-Wesley Publishing Company, 1993.

[9] X. Huang, P. Jiang, C. Kim, Q. Ke and G. Wang, "Preparation, microsctrucutre and properties of polyethylene aluminum nanocomposite dielectrics," *Composites Science and Technology,* vol. 68, pp. 2134-2140, 2008.

[10] G. Sui, S. Jana, W. Zhong, M. Fuqua and C. Ulven, "Dielectric properties and conductivity of carbon nanofiber/semi-crystalline polymer composites," *Science Direct,* vol. 56, pp. 2381-2388, 2008.

[11] H. G. Karian, Handbook of Polypropylene and Polypropylene Composites, Basel, Switzerland: Marcel Dekker, Inc, 1999.

[12] S. Wang, J. Zhang, S. Chen and H. Zhu, "Crystal structure and melting behavior of homo-polypropylene and heterophasic ethylene-propylene copolymer after long heat treatment," *Journal of Crystal Growth,* vol. 355, pp. 151-158, 2012.

[13] B. Lotz, "α and β phases of isotactic polyproylene: a case of growth kinetics 'phase reentrency' in polymer crystallizaton," *Polymer,* vol. 39, pp. 4561-4567, 1998.

[14] V. Jozsef, "β-modification of isotactic polypropylene: preparation, structure, processing, properties, and application," *Journal of Macromolecular science, Part B: Physics,* vol. 41, no. 4-6, pp. 1121-1171, 2007.

[15] K. Nozaki, Y. Endo, T. Yamamoto and M. Naiki, "Crystallization of α and β phases in isotactic polypropylene with low ethylene content: Isothermal crystallization and secondary crystallization," Yamaguchi University, Yamaguchi, Japan.

[16] J. Varga, I. Mudra and G. W. Ehrenstein, "Crystallization and melting of β-nucleated isotactic polypropylene," *Journal of Thermal Analysis and Calorimetry,* vol. 56, pp. 1047-1057, 1999.

[17] S. Wang and J. Zhang, "Effects of nucleating agent on the crystallization behavor, crystal form and solar reflectance of polypropylene," *Solar energy materials & solar cells,* vol. 117, pp. 577-584, 2012.

[18] Y. Li, S. Wang, Y. Zhang and Y. Zhang, "Crystallization Behavior of Carbon Black-Filled Polypropylene and Polypropylene/Epoxy Composites," Research Institute of Polymer Materials, Shanghai, 2005.

[19] R. F., "Orientation in Composite of Polypropylene and Talc," Technical University Brno, Gottwaldov, 1988.

[20] G. W. Ehrenstein, G. Riedel and P. Trawiel, Thermal Analysis of Plastics, Hanser, 2004.

[21] D. R. Bowman and D. G. Stroud, "Model for dielectric breakdown in metal-insulator composites," *Physical Review B.,* pp. 4641-4650, 1989.

[22] F. Kremer and A. Schönhals, Broadband Dielectric Spectroscopy, Berlin: Springer-Verlag, 2003.

[23] A. Eriksson, L. Beilina and T. M. Larsen, "Reconstructionofannularbi-layered mediaincylindricalwaveguidesection," *Journal of Mathematics in Industry,* 2017.

[24] R. E. Collin, Foundations for Microwave Engineering, McGraw Hill, 1992.

[25] D. Ghodgaonkar, V. Varadan and V. Varadan, "Free-Space Measurement of Complex Permittivity and Complex Permeability of Magnetic Materials at Microwave Frequencies," *IEEE Transactions on Instrumentation and Measurement,* vol. 39, no. 2, pp. 387-394, 1990.

[26] A. A. Tracton, Coatings Technology: Fundamentals, Testing, and Processing Techniques, CRC Press, 2006.

[27] D. H. Im and E. S. Kim, "Effects of Crystallinity on Dielectric Properties of MgWO4 Filled Semi-Crystalline Polymer Composites," *Ferroelectrics,* vol. 434, pp. 19-26, 2012.

[28] O. Hashimoto, H. Higashi and K. Orikabe, "Measurement of Complex Permittivity of Radome Material at 60 GHz Frequency Ban," *Electronics and Communications in Japan,* vol. 82, no. 12, pp. 906-911, 199.

[29] R. Schnabel, D. Mittelstraß, T. Binzer, C. Waldscmidt and R. Weigel, "Reflection, Refraction, and Self-Jamming," *IEEE Microwave Magazine,* pp. 107-117, 2012.

[30] W. C. Johnson, "Transmission Lines and Networks," McGraw-Hill, 1963, p. 58.

[31] W. Groenewoud, "Characterization of Polymers by Thermal Analysis," 2001, p. 26.

[32] J.-B. Kim, S.-K. Lee and C.-G. Kim, "Comparison study on the effect of carbon nano materials for single-layer microwave absorbers in X-band," *Composites Science and Technology,* vol. 68, pp. 2909-2916, 2008.

[33] F. Fitzek, R. Rasshofer and E. Biebl, "Comparison of matching layers for automotive radome design," *Advances in Radion Science,* vol. 8, pp. 49-54, 2010.

[42] D. Forslund and J. Bjärkefur, "Night Vision Animal Detection," in *IEE Intelligent Vehicles Symposium*, Dearborn, Michigan, USA, 2014.

A: Sample information

Table 9: Plastic substrate sample information

Plastic substrate	Composition	Comment
PP_1	100 % PP	
PP_2	PP, 30 % Talc (Large, flat flakes), unknown % CB	Never received this sample
PP_3	PP, 15 % Talc (fine-grained) and unknown % CB	
PP_4	PP, 15 % Talc (fine-grained) and 0,5 % CB	
PP_5	PP, 20 % Talc and 0,6 % CB	
PP_6	PP, 20 % Talc and unknown % metal flakes	Assumed high reflection
PP_7	PP, composition unknown	Radar absorbing material
PP_8	PP, 15 % Talc and unknown % CB	
PP_9	PP, 20 % Talc and unknown % CB	
PP_{10}	Unknown composition	

Table 10: Primer sample information

Primer	Thickness	Comment
Pr_1	4 µm	
Pr_2	4 µm	
Pr_3	30-35 µm	CPO mixed with basecoat $BC_{7.1}$
Pr_4	-	

Table 11: Basecoat sample information

Basecoat	Thickness	Type	Composition	Comment
BC_1	15 µm	Effect pigment	6.24 % Al (SD 24 µm & CF 8-29 µm)	
BC_2	30 µm	Solid		
BC_3	15 µm	Effect pigment	6.41 % Al (SD 4-26 µm)	

BC_4	15 µm	Effect pigment	Xirallic 0,2 % (2-30 µm)	
BC_5	15 µm	Effect pigment	0,7 % Al (CF 18-53µm 0,1%, SD 11-32µm 0,5%, SD 4-21µm 0,1%) Mica 5-25µm 0,5%, Mica 5-40µm 0,4%)	
BC_6	10 µm	Solid		
$BC_{7.2}$	10 µm	Effect pigment	No metal content but other unknown effect pigmentation	
BC_8	-	PVD-coating	Unknown metal	
BC_9	-	Effect pigment	-	The same colour as CB_1, different supplier. Composition might differ.
BC_{10}	-	Effect pigment	-	The same colour as CB_1, different supplier. Composition might differ.

Table 12: Clearcoat sample information

Clear Coat	Thickness
CC_1	40 µm
CC_2	40 µm
CC_3	-
CC_4	

Table 13: Measured coating thicknesses for all coated samples

Sample	Primer [µm]	Base Coat 1 [µm]	Top Coat 1 [µm]	Base Coat 2 [µm]	Top Coat 2 [µm]	Base Coat 3 [µm]	Top Coat 3 [µm]
S9_1	4	-	-	-	-	-	-
S9_2	4	-	-	-	-	-	-
S10_1	4	23,53	-	-	-	-	-
S10_2	4	25,73	-	-	-	-	-
S11_1	4	22,85	33,150	-	-	-	-
S11_2	4	25,560	27,727	-	-	-	-
S12_1	4	24,330	47,220	20,213	48,913	-	-
S12_2	4	23,373	35,870	21,697	45,297	-	-
S13_1	4	33,593	31,663	-	-	-	-
S13_2	4	35,040	28,093	-	-	-	-
S14_1	4	19,166	35,010	-	-	-	-
S14_2	4	21,430	36,070	-	-	-	-
S15_1	4	16,250	35,337	-	-	-	-
S15_2	4	19,550	27.275	-	-	-	-
S16_1	4	27,520	34,750	-	-	-	-
S16_2	4	x	x	-	-	-	-
S17_1	4	25,747	35,510	-	-	-	-
S17_2	4	22,140	30,513	-	-	-	-
S18_1	38,94	9,883	36,703	-	-	-	-
S18_2	40,837	9,557	31,890	-	-	-	-
S19	-	48,547	-	-	-	-	-
S20_1	4	22,650	30,277	24,783	60,980	-	-
S20_2	4	23,333	28,640	23,657	59,703	-	-
S21_1	4	23,780	28,037	23,043	61,663	19,927	53,627
S21_2	4	21,400	29,923	22,360	63,177	21,883	52,627
S22_1	4	18,570	31,440	25,420	60,397	-	-
S22_2	4	22,040	31,047	27,517	64,353	-	-
S23_1	4	19,027	37,633	25,767	62,923	17,153	48,693
S23_2	4	23,303	37,810	23,970	61,31	16,733	48,750
S24_1	-	-	-	-	-	-	-
S24_2	-	-	-	-	-	-	-
S25_1	4	-	-	-	-	-	-
S25_2	4	-	-	-	-	-	-
S26_1	5,917	-	41,703	-	-	-	-
S26_2	5,790	-	39,757	-	-	-	-

B: Plastics substrates

Table 14: TGA components all samples. S# is the number of the sample, the number after is the number of the plate of the same sample, and extra means an extra measurement was done on the plate

```
     Sample         Water      PolymerMatrix    CarbonBlack     Talc_InertMaterial
    ____________    ______    _____________    ___________    __________________

    'S1_1'           0.282    99.282           -0.5061          0.9417
    'S1_1_extra'    0.2584    99.155           -0.1477          0.7342
    'S1_2'          0.3561    99.127           -0.5936          1.1102
    'S1_2_extra'    0.1907    99.662           -0.5908          0.7376
    'S3_1'          0.4607    50.224            1.1971          48.118
    'S3_2'          0.4922    50.214            1.2423          48.052
    'S4_1'          0.6415    83.412            0.5665          15.381
    'S4_2'          0.6626    83.363            0.7344           15.24
    'S5_1'          0.5325    77.904            0.8697          20.694
    'S5_1_extra'    0.8037    77.946            0.5341          20.716
    'S5_2'          0.5049    76.471            1.0057          22.019
    'S6_1'          0.9777    74.823            0.0188          24.181
    'S6_2'          0.9396     74.87            0.0027          24.187
    'S7_1'          0.8236     79.39            19.343          0.4435
    'S7_1_extra'    0.3993     79.86            19.402          0.3392
    'S7_2'          0.3884    79.297            19.486          0.8289
    'S8_1'          0.4797    65.755            0.7033          33.062
    'S8_1_extra'    0.7321    65.822             0.601          32.845
    'S8_2'          0.3698    72.222            0.6227          26.785
    'S8_2_extra'    0.4614    73.294            0.8547           25.39
    'S19'           1.0476     88.06            10.659          0.2333
    'S19_extra'     1.2565    88.763             10.48         -0.4992
    'S24_1'         0.6618    74.257            2.4322          22.649
    'S24_2'         1.0226    74.801            2.3595          21.817
```

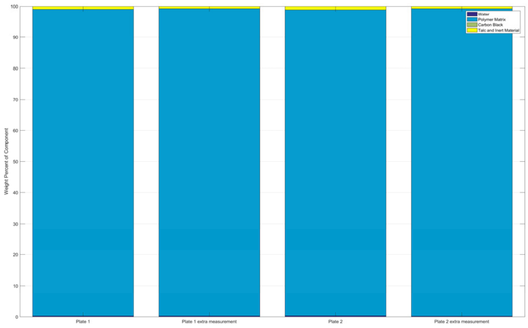

Figure 42: Composition of Sample 1 Plates

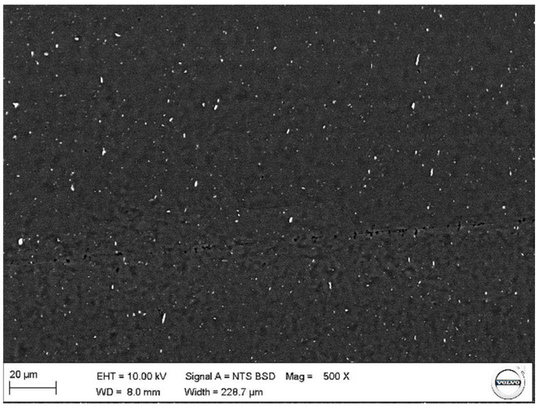

Figure 43: BS SEM image of sample 1 at 500x magnification

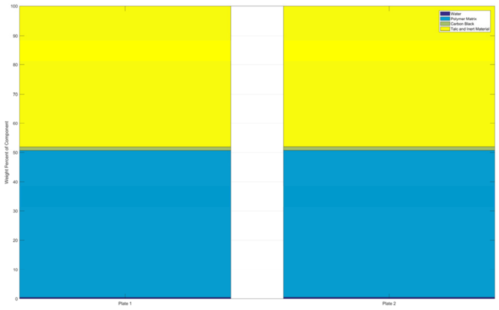

Figure 44: Composition of Sample 3 Plates

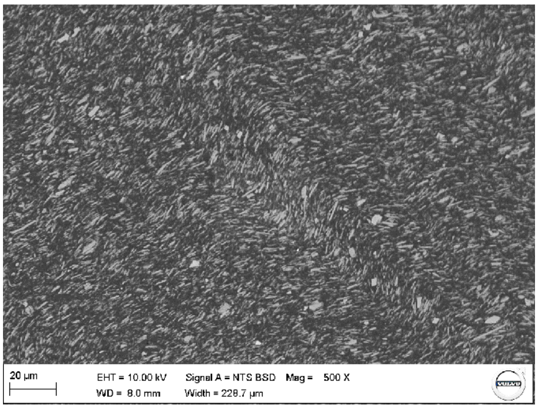

Figure 45: BS SEM image of sample 3 at 500x magnification

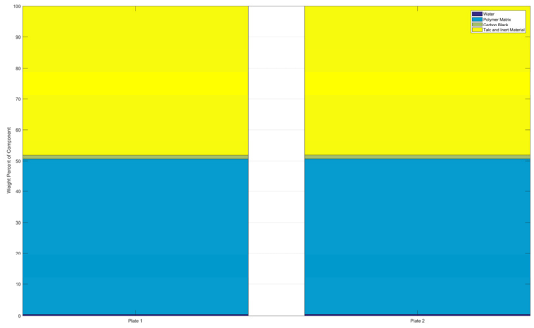

Figure 46: Composition of Sample 4 Plates

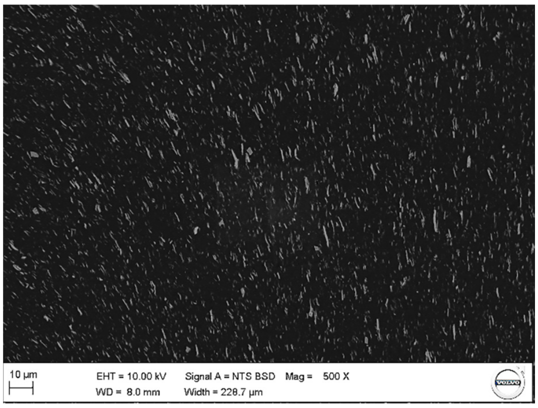

Figure 47: BS SEM image of sample 4 at 500x magnification

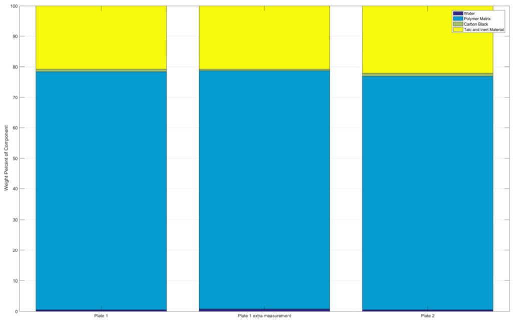

Figure 48: Composition of Sample 5 Plates

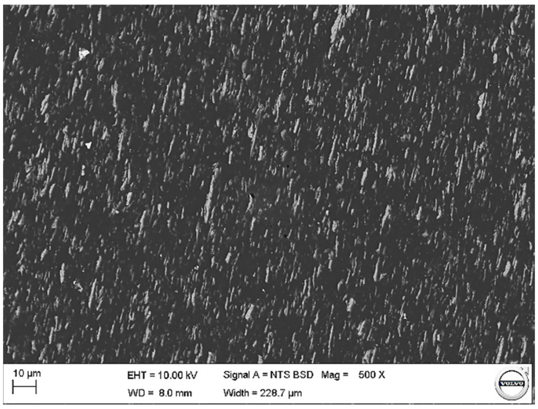

Figure 49: BS SEM image of sample 5 at 500x magnification

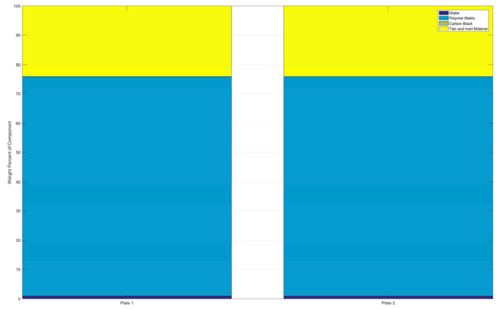

Figure 50: Composition of Sample 6 Plates

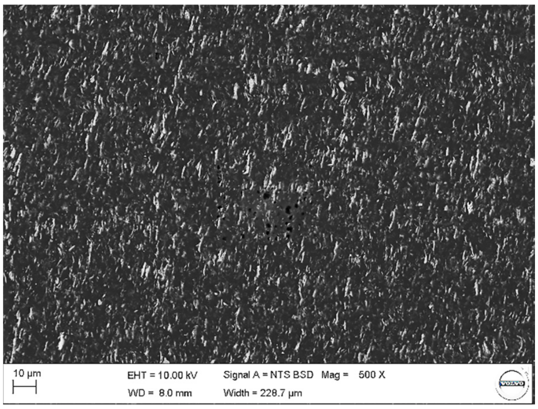

Figure 51: BS SEM image of sample 6 at 500x magnification

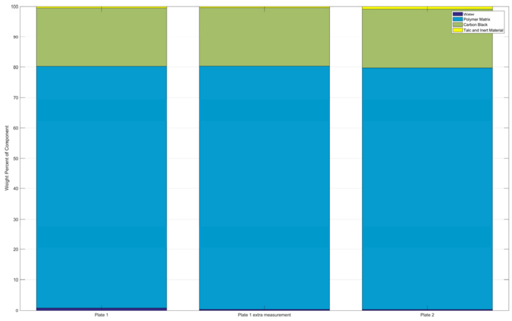

Figure 52: Composition of Sample 7 Plates

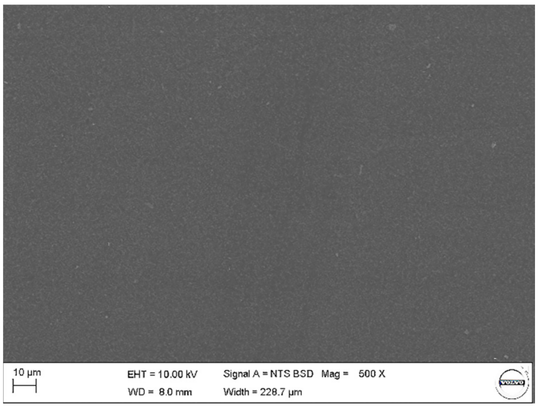

Figure 53: BS SEM image of sample 7 at 500x magnification

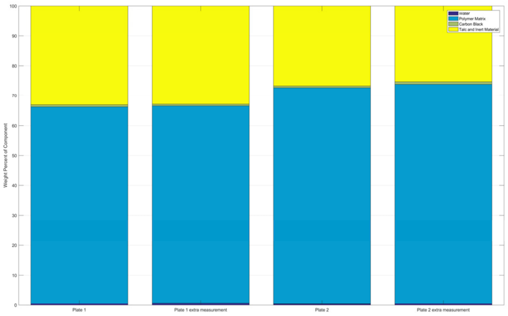

Figure 54: Composition of Sample 8 Plates

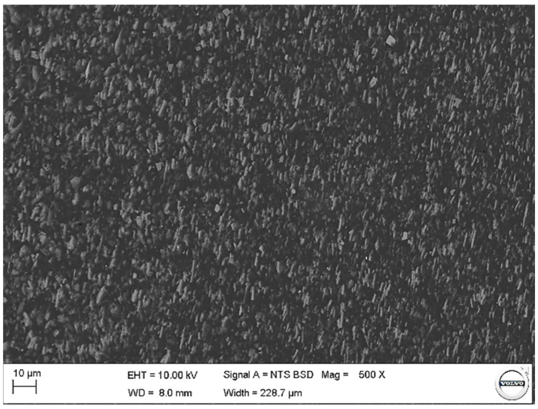

Figure 55: BS SEM image of sample 8 at 500x magnification

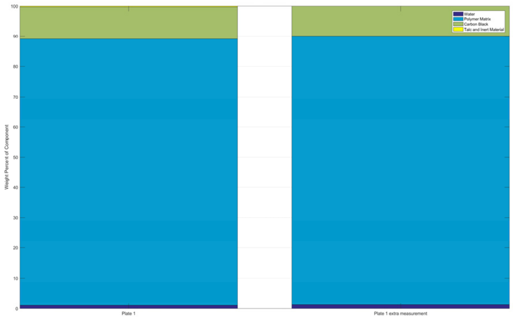

Figure 56: Composition of Sample 19 Plates

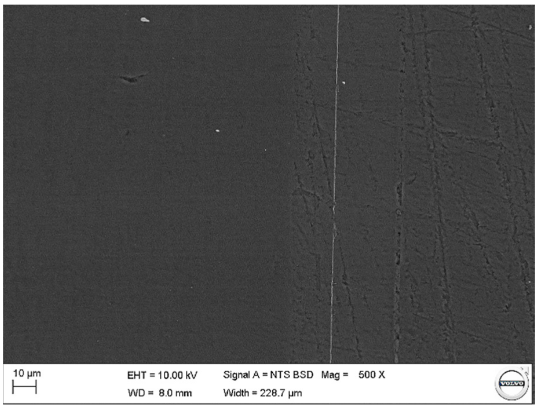

Figure 57: BS SEM image of sample 19 at 500x magnification

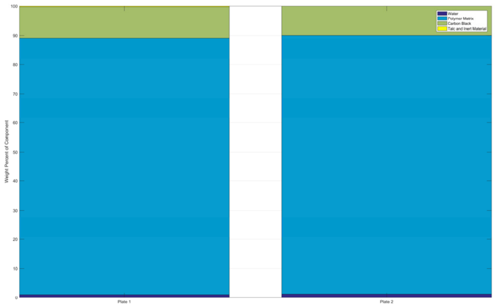

Figure 58: Composition of Sample 24 Plates

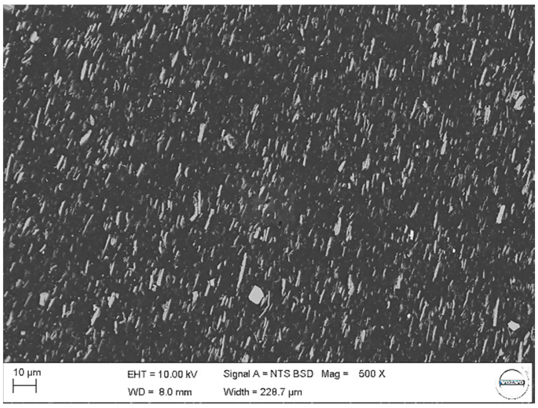

Figure 59: BS SEM image of sample 24 at 500x magnification

Table 15: TGA derivatives all samples. S# is the number of the sample, the number after is the number of the plate of the same sample, and extra means an extra measurement was done on the plate.

Sample	Derivative
'S1_1'	0.7
'S1_1_extra'	0.68
'S1_2'	0.71
'S1_2_extra'	0.71
'S3_1'	0.45
'S3_2'	0.44
'S4_1'	0.61
'S4_2'	0.6
'S5_1'	0.55
'S5_1_extra'	0.57
'S5_2'	0.57
'S6_1'	0.51
'S6_2'	0.51
'S7_1'	0.78
'S7_1_extra'	0.73
'S7_2'	0.8
'S8_1'	0.56
'S8_1_extra'	0.56
'S8_2'	0.63
'S8_2_extra'	0.64
'S19'	0.27
'S19_extra'	0.45
'S24_1'	0.58
'S24_2'	0.58

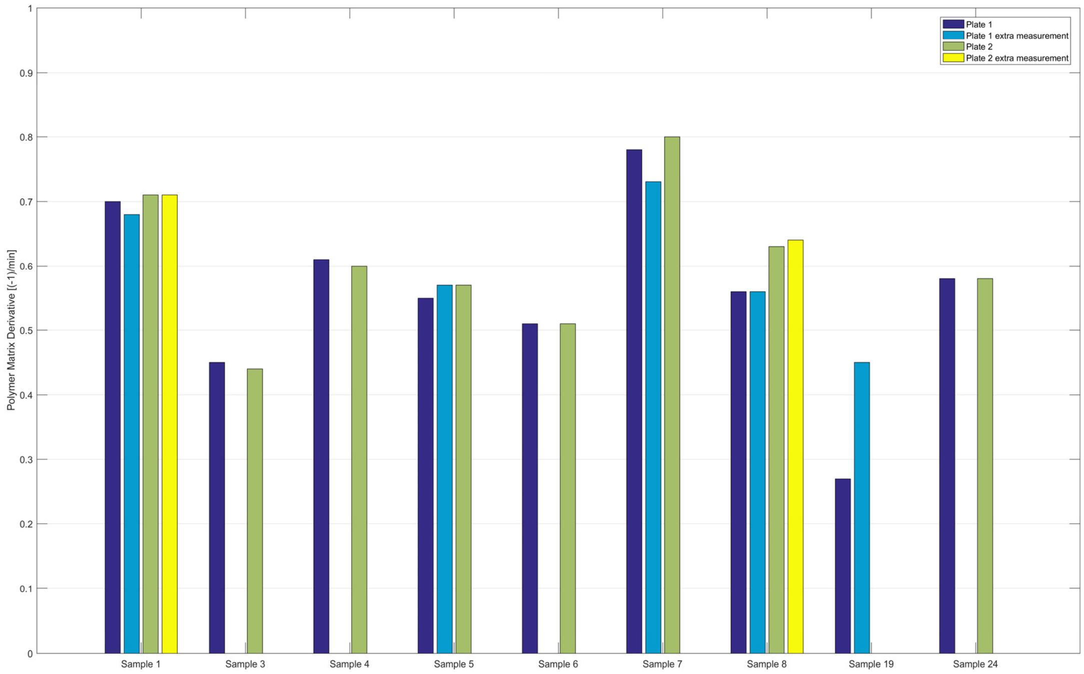

Figure 60: TGA samples derivatives

C: MATLAB modelling of aftermarket painted samples

```
eps=[1 4-0.1j 2 1];% Relative permittvity of two layer dielectric in free
space
thick=[5 2];   %Thickess in mm
freq=linspace(70,80,1601);  % Frequency in GHz
pol='te';   %Polarization 'te' or 'tm'
theta=20;   %Anglein degrees
[Gamma Z]=multidielGHzmm(eps,thick,freq,theta,pol);
Reflection=abs(Gamma).^2;

figure, plot(freq,Reflection)
xlabel('Freq(GHz)')
legend('Reflection')
box off
```

```
function [ref,Z] = multidielGHzmm(eps,thick,freq,theta,pol)
%if nargin==0, help multidiel; return; end
if nargin<=4, pol='te'; end
if nargin==3, theta=0; end

n = sqrt(eps);
la = 300./freq;
opthick = thick.*n(2:length(n)-1);
[ref,Z] = multidiel(n,opthick,la,theta,pol);
```

```
% multidiel.m - reflection response of isotropic or birefringent multilayer
structure
%
%          na | n1 | n2 | ... | nM | nb
% left medium | L1 | L2 | ... | LM | right medium
%   interface 1    2    3     M   M+1
%
% Usage: [Gamma,Z] = multidiel(n,L,lambda,theta,pol)
%        [Gamma,Z] = multidiel(n,L,lambda,theta)       (equivalent to
pol='te')
%        [Gamma,Z] = multidiel(n,L,lambda)             (equivalent to
theta=0)
%
% n      = isotropic 1x(M+2), uniaxial 2x(M+2), or biaxial 3x(M+2), matrix
of refractive indices
% L      = vector of optical lengths of layers, in units of lambda_0
% lambda = vector of free-space wavelengths at which to evaluate the
reflection response
% theta  = incidence angle from left medium (in degrees)
% pol    = for 'tm' or 'te', parallel or perpendicular, p or s,
polarizations
%
% Gamma = reflection response at interface-1 into left medium evaluated at
lambda
% Z     = transverse wave impedance at interface-1 in units of eta_a (left
medium)
%
% notes: M is the number of layers (M >= 0)
%        n = [na, n1, n2, ..., nM, nb]        = 1x(M+2) row vector of
isotropic indices
%
%            [ na1  n11  n12  ...  n1M  nb1 ]   3x(M+2) matrix of
birefringent indices,
```

```
%        n = [ na2  n21  n22  ...  n2M  nb2 ] = if 2x(M+2), it is extended
to 3x(M+2)
%            [ na3  n31  n32  ...  n3M  nb3 ]   by repeating the top row
%
%        optical lengths are in units of a reference free-space wavelength
lambda_0:
%        for i=1,2,...,M,  L(i) = n(1,i) * l(i), for TM,
%                          L(i) = n(2,i) * l(i), for TE,
%        TM and TE L(i) are the same in isotropic case. If M=0, use L=[].
%
%        lambda is in units of lambda_0, that is, lambda/lambda_0 = f_0/f
%
%        reflectance = |Gamma|^2, input impedance = Z = (1+Gamma)./(1-
Gamma)
%
%        delta(i) = 2*pi*[n(1,i) * l(i) * sqrt(1 - (Na*sin(theta))^2 ./
n(3,i).^2))]/lambda, for TM
%        delta(i) = 2*pi*[n(2,i) * l(i) * sqrt(1 - (Na*sin(theta))^2 ./
n(2,i).^2))]/lambda, for TE
%
%        if n(3,i)=n(3,i+1)=Na, then will get NaN's at theta=90 because of
0/0, (see also FRESNEL)
%
%        it uses SQRTE, which is a modified version of SQRT approriate for
evanescent waves
%
%        see also MULTIDIEL1, MULTIDIEL2

% Sophocles J. Orfanidis - 1999-2008 - www.ece.rutgers.edu/~orfanidi/ewa

function [Gamma,Z] = multidiel(n,L,lambda,theta,pol)

if nargin==0, help multidiel; return; end
if nargin<=4, pol='te'; end
if nargin==3, theta=0; end

if size(n,2)==1, n = n'; end                            % in case n is
entered as column

K = size(n,1);                                          % birefringence
dimension
M = size(n,2)-2;                                        % number of layers

if K==1, n = [n; n; n]; end                             % isotropic case
if K==2, n = [n(1,:); n]; end                           % uniaxial case

if M==0, L = []; end                                    % single interface,
no slabs

theta = theta * pi/180;

if pol=='te',
    Nsin2 = (n(2,1)*sin(theta))^2;                      % (Na*sin(tha))^2
    %c = conj(sqrt(conj(1 - Nsin2 ./ n(2,:).^2)));      % old version
    c = sqrte(1 - Nsin2 ./ n(2,:).^2);                  % coefficient ci,
or cos(th(i)) in isotropic case
    nT = n(2,:) .* c;                                   % transverse
refractive indices
    r = n2r(nT);                                        % r(i) = (nT(i-1)-
nT(i)) / (nT(i-1)+nT(i))
```

```
else
    Nsin2 = (n(1,1)*n(3,1)*sin(theta))^2 / (n(3,1)^2*cos(theta)^2 +
n(1,1)^2*sin(theta)^2);
    %c = conj(sqrt(conj(1 - Nsin2 ./ n(3,:).^2)));
    c = sqrte(1 - Nsin2 ./ n(3,:).^2);
    nTinv = c ./ n(1,:);                                % nTinv(i) =
1/nT(i) to avoid NaNs
    r = -n2r(nTinv);                                    % minus sign
because n2r(n) = -n2r(1./n)
end

if M>0,
    L = L .* c(2:M+1);                                  % polarization-
dependent optical lengths
end

Gamma = r(M+1) * ones(1,length(lambda));                % initialize Gamma
at right-most interface

for i = M:-1:1,                                         % forward layer
recursion
    delta = 2*pi*L(i)./lambda;                          % phase thickness
in i-th layer
    z = exp(-2*j*delta);
    Gamma = (r(i) + Gamma.*z) ./ (1 + r(i)*Gamma.*z);
end

Z = (1 + Gamma) ./ (1 - Gamma);
```

C.1. Sample 20

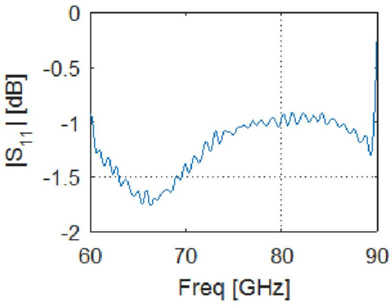

Figure 61: S11 measurement from free-space method on sample S20_1.

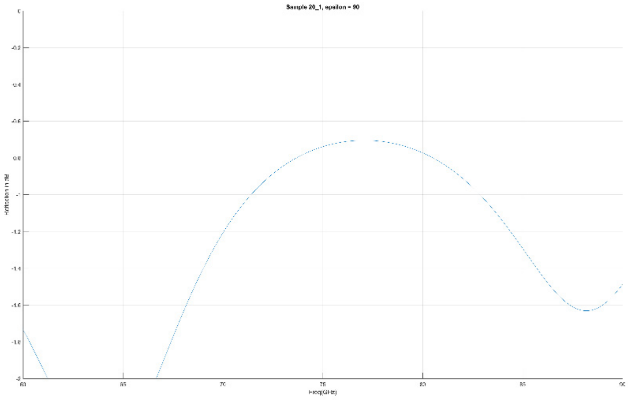

Figure 62: Modelling of sample S20_1 dielectric constant using multidiel.m in Matlab.

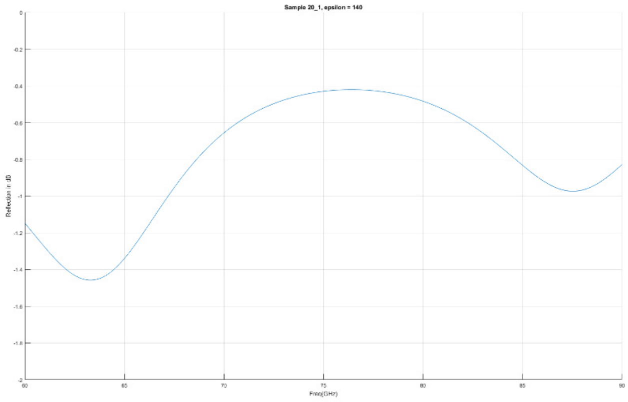

Figure 63: Modelling of sample S20_1 dielectric constant using multidiel.m in Matlab.

C.2. Sample 21

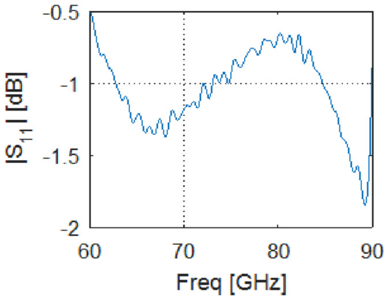

Figure 64: S11 measurement from free-space method on sample S21_1.

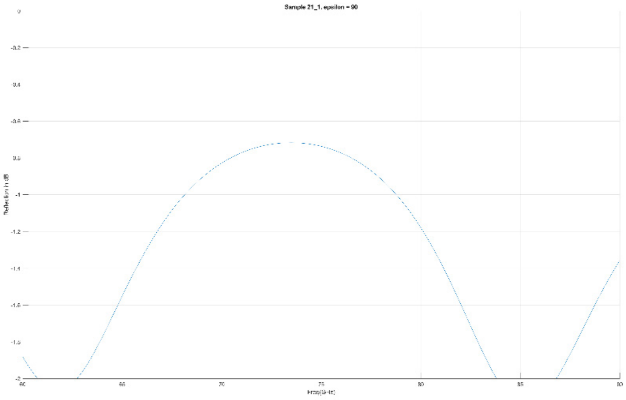

Figure 65: Modelling of sample S21_1 dielectric constant using multidiel.m in Matlab.

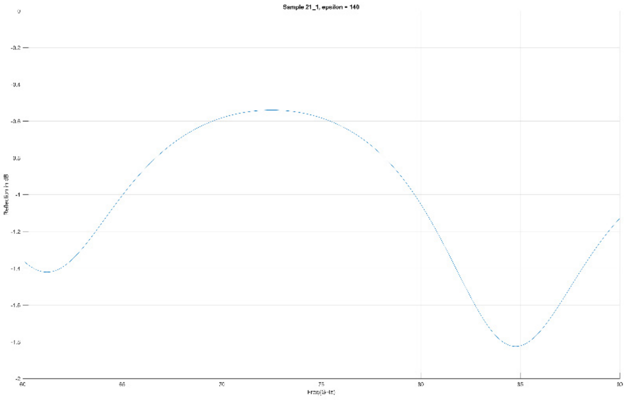

Figure 66: Modelling of sample S21_1 dielectric constant using multidiel.m in Matlab.

C.3. Sample 22

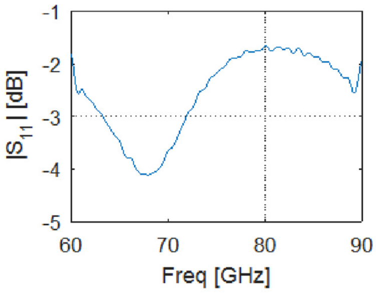

Figure 67: S11 measurement from free-space method on sample S22_1.

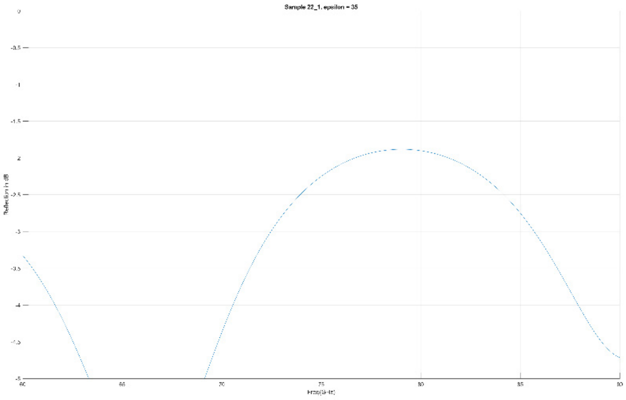

Figure 68: Modelling of sample S22_1 dielectric constant using multidiel.m in Matlab.

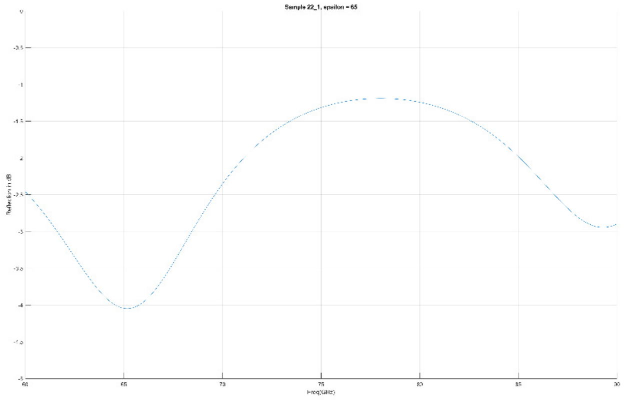

Figure 69: Modelling of sample S22_1 dielectric constant using multidiel.m in Matlab.

C.4. Sample 23

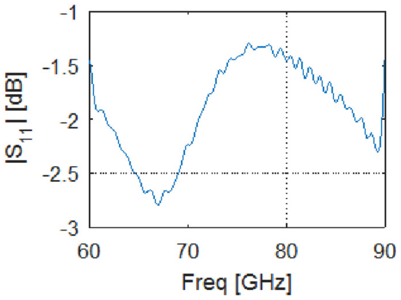

Figure 70: S11 measurement from free-space method on sample S23_1.

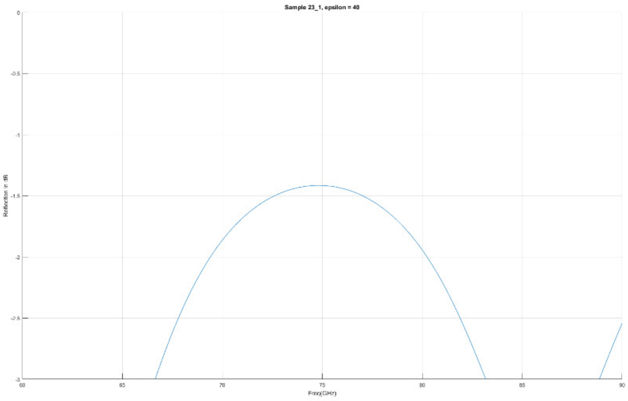

Figure 71: Modelling of sample S23_1 dielectric constant using multidiel.m in Matlab.

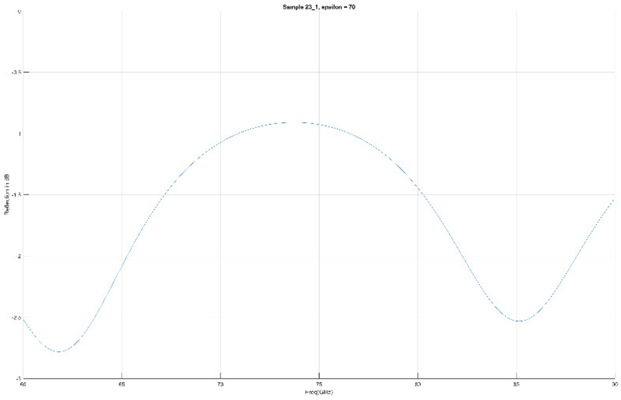

Figure 72: Modelling of sample S23_1 dielectric constant using multidiel.m in Matlab.